

The effect of intraspecific variation in calcaneal tuber length on endurance running economy

A biomechanical perspective on human evolution using 3D predictive simulations and Optimization theory in OpenSim/MATLAB

Authors:

Maarten Beijleveld¹

Supervisor

First supervisor: Jelle Reumer²

Second supervisor: Jaap van Dieen³

Abstract

Intraspecific- and interregional variation in human endurance running performance are both long studied topics. Endurance running is defined as the ability to run long distances ($5 > \text{km}$) using aerobic metabolism. As today, athletes from East Africa dominate endurance running competitions, the proposed reasons for the observed variations are numerous and in some cases ethically questionable. As today, no consensus exists on the matter. The answer as to why humans are efficient endurance runners at all, as opposed to many other mammals, can be found in the rich literature concerning human evolution. The process of human feet evolution especially has led to the development of specific traits that enhance endurance running; these traits emerge after the divergence between Chimpanzees and the ancestral hominin. This paper focuses on the Achilles tendon moment arm as specific variable trait that may affect endurance running performance. The fossil record provides evidence for the transition from arboreality to bipedal walking and endurance running, in the form of fossil morphology and trackways. Early hominins, such as the *Australopithecines*, are thought to represent the transition between arboreality and bipedal walking, while *Homo erectus* is thought to be the first capable of endurance running. The main selection pressure for endurance running is related to the persistence hunting theory. The persistence hunting theory states that the human thermoregulatory efficiency, combined with increased musculoskeletal efficiency would enable early hominins to hunt prey to exhaustion. Early hominins adapted musculoskeletal and thermoregulatory traits that would favor persistence hunting and grant first access to prey. One such musculoskeletal trait is the Achilles tendon, the Achilles tendon behaves as an elastic spring, in which energy can be stored and reutilized. The amount of energy stored in the Achilles tendon is a function of mainly the Achilles tendon moment arm length. A fossil proxy for Achilles tendon moment arm is the calcaneal tuber length. In this paper it is hypothesized that a smaller tuber increases the energy storage in the Achilles tendon and reduces the cost of transport (J/kg/m) of endurance running at 4 m/s. Calcaneal tuber length was measured on two sample groups (Haya, Kenya and Sedgeford, England) to evaluate intraspecific but also interregional differences in cost of transport for running at 4 m/s. The Kenyan group as opposed to the English group demonstrated a statistically significant smaller average calcaneal tuber lengths, $t(32) = 1.69$, $p =$

¹ Utrecht University, Geosciences, Earth Life & Climate

² Utrecht University, Vertebrate Paleontology

³ Vrije Universiteit Amsterdam, Human Movement Sciences

0.026. This experimental data was implemented in the biomechanical software program OpenSim, and combined with optimization theory in MATLAB. 3D predictive simulations were performed to test the hypothesis. Predictive simulations, as opposed to non-predictive simulations allow both the kinematics and kinetics to change due to a change in calcaneal morphology. Sensitivity experiments were performed to evaluate the effect of scaling, locomotive speed, tendon stiffness and initial guess mode. Due to limited sample control, no conclusions can be based on interregional differences. Based on maximal observed difference in calcaneal tuber length (0.338 cm), a smaller calcaneum reduces the cost of transport with 4.5% at 4 m/s and 0.78% at 1.33 m/s. The reduction in cost of transport is attributed to a reduction muscle energy consumption of the peroneus brevis and peroneus longus muscles. No significant relationship was found between tendon energy storage in the Achilles tendon and calcaneal length. The scaling procedure proved to have limited effect on the triceps surae muscle tendon unit. A more compliant tendon (20 N/cm instead of 35 N/cm) resulted in lower cost of transport for running and higher cost of transport for walking. The fossil record is too fragmentary to provide any conclusive evidence on calcaneal evolution. It appears that the general foot evolution is directional towards enhanced bipedalism, but that for specific endurance running either many reversals occurred or that hominin species developed specific traits individually.

Foreword

Johnny Salo completed the transcontinental race in 1929 from New York to Los Angeles in 525 hours, 56 minutes and 10 seconds with an average of 8.53 minutes per mile for over 3500 miles⁴.

Man VS horse, a peculiar bet led to a peculiar record. In 2004 Huw Lobb competed with a horse on the marathon and won by 2 minutes⁵.

Running 15km to kill an antelope through exhaustion requires fewer calories than the consumption of a Big Mac and medium sized fries⁶

34 year old Kenyan athlete Eliud Kipchoge became the first athlete to complete the marathon within 2 hours with an average speed of 5.8 m/s⁷.

These amazing accomplishments are the reason for my unbounded interest in movement science and general anthropology. They are a testament for the story of human evolution and show that the boundaries to human locomotion can always be tested and extended to enormous limits. This paper tries to contribute to our current knowledge on human locomotion.

⁴ <https://www.runnersworld.com/advanced/a20813682/the-1929-great-transcontinental-footrace/>

⁵ <http://www.man-v-horse.org.uk/>

⁶ Lieberman, D.E., et al., *Brains, brawn, and the evolution of human endurance running capabilities*, in *The first humans—origin and early evolution of the genus homo*. 2009, Springer. p. 77-92.

⁷ <https://time.com/5707230/eliud-kipchoge/>

Table of contents

Abstract	1
Foreword	2
Table of contents	3
1. Introduction	4
2. Background	8
2.1 <i>History of human locomotion</i>	8
The origin of bipedal walking and running	9
Natural selection pressure for bipedal walking and running	10
The evolution of the human foot	12
2.2 <i>Biomechanics of human locomotion</i>	15
Functional anatomy	15
Biomechanical description of locomotion	17
Biomechanics of the human foot	22
3. Methods	24
3.1 <i>Data collection</i>	24
3.2 <i>Predictive simulations</i>	25
4. Results	29
4.1 <i>Endurance running</i>	30
4.2 <i>Walking</i>	33
5. Discussion	36
5.1 <i>Optimization performance</i>	36
5.2 <i>Results</i>	38
5.3 <i>Endurance running evolution</i>	41
Conclusion	43
Acknowledgements	44
Works Cited	44

1. Introduction

Marathon running is categorized as endurance running, which is defined as the ability to run long distances ($5 > \text{km}$) using aerobic metabolism. Humans are exceptionally good at endurance running with endurance running speeds often exceeding 2.5 m/s (9 km/h) and reaching up to 6.5 m/s (23 km/h) in elite athletes. Humans even have the capability to outrun most other mammals on marathon-length distances [2]. Within modern humans large differences in endurance running performance are observed, with differences between individuals (intraspecific) but also differences based on region (interregional). Currently East African athletes mainly from Kenya and Ethiopia outperform most other athletes on endurance running competitions [IAAF⁸] [3]. The Kenyan Kalenjin tribe for example has won most of the Olympic medals for Kenya on endurance running competitions. The dominance of East African athletes is relatively recent considering that about four decades ago Europeans dominated the marathon competition [3]. If endurance running performance is considered outside of large competitions, the Mexican Tarahumara Indians are also well known for long distance running capabilities [4]. The scientific fields of Anthropology and Biomechanics have long tried to understand why humans are so exceptionally good at endurance running, and what may cause intraspecific variation in endurance running performance. As today no paradigm exists on the matter. This paper will, by means of literature research and biomechanical simulations, contribute to the understanding of intraspecific variation in endurance running performance.

Running and walking are the two typical locomotive styles of humans; both types of locomotion have deep roots in human evolution. In the context of human evolution, the exceptional ability of humans to run long distances is strange; humans (*Homo sapiens*) belong to the Order Primates and no other genus within this Order shows the same bipedal performance on long distance running. Most modern primates are mainly arboreal, and move quadrupedal on terrestrial grounds. These primates have many specializations that improve performance capabilities for climbing that limit locomotive performances; also the energetic cost of human endurance running is relatively high when compared with human walking and other mammalian gaits. Humans belong to the family Hominidae (hereafter called hominids), which includes all modern and extinct Great Apes. Within this family *Homo sapiens* belong to the tribe Hominini (hereafter called hominins) which constitutes a group of modern and extinct humans and our immediate ancestors. This distinction in nomenclature separates the first 'human like' ancestors such as the *Australopithecines* from the ancestral 'ape ancestor' that is shared with the chimpanzee, orangutan and gorilla. Divergence between chimpanzees and the earliest hominin occurred around 7 million years ago, and evident bipedalism dates back to 3.6 million years ago [5]. According to the fossil record endurance running (ER) capabilities first evolved around 1.9 million years ago with the emergence of *Homo erectus* [1, 2, 6]. Various morphological traits have developed since the divergence of chimpanzees and early hominins (see table 1, and Bramble & Lieberman [1]). Different selection pressures must have been responsible for the development of specific traits for walking and running and the development of specific traits may explain the intraspecific variation seen in human endurance running performance.

⁸ IAAF All Time Outdoor Time Top List (<https://www.worldathletics.org/records/all-time-toplists/road-running/marathon/outdoor/men/senior>)

To understand why against all odds humans are so exceptionally good at endurance running, a combination of scientific disciplines is required. In this paper this broad question is initially approached from the perspective of human evolution. Human evolution sheds light on why and when early hominids became bipedal and how this relates to endurance running. This broad question will be answered by means of literature research and forms part of the background information. The main research question of this paper specifies on a single morphologic trait which affects endurance running performance. This specific trait is the calcaneal tuber length and its relationship with the Achilles muscle tendon unit. Does intraspecific variation in calcaneal tuber length affect the metabolic energy expenditure (J/kg/ m) of endurance running? It is hypothesized that intraspecific variation in calcaneal morphology resulting in a smaller calcaneal moment arm length can decrease endurance running energy expenditure and thereby improve endurance running performance. It may in part explain the dominance of East African athletes in endurance running competitions. A sub question is: does the fossil record show change in calcaneal morphology over evolutionary timescales that would indicate enhanced running performance? 3D predictive simulations in OpenSim in combination with optimization theory in MATLAB will be applied to evaluate the effect of intraspecific differences in calcaneal morphology on endurance running performance, these simulations also provide means to evaluate the relationship between metabolic energy expenditure and calcaneal tuber length. Predictive simulations are chosen over other simulative methods since it is expected that kinematics and kinetics both change due to different dimensions of the calcaneum. Other simulative methods use experimental data on kinematics, and kinematics do not change during the course of a simulation. The calcaneal material is available from the Duckworth Laboratory in Cambridge⁹, recent material from the Haya people of Kenya will be compared with recent material from Saxon graves of England (Sedgeford). Since this paper discusses intraspecific variation in endurance running based on ethnicity, the following statement is included:

The question concerning intraspecific variation in endurance running performance can be approached from multiple scientific viewpoints, and from the social aspect this question often leads to racial ethnic debates. The social aspect concentrates on the (often wrongly assumed) cultural historical development of East Africa. Slavery was justified in part by arguments that Africans were specialized in physical labor, and whites in mental work. These ideas still persist in modern racism. Talking about physical attributes of colored men and women without any awareness of this eminent social aspect may echo some of the worst moments of modern history. I am as a white scientist talking about an East African ethnic group. By no means, this paper justifies or implies racial discrimination. This paper will enhance our current insight in the beautiful story of human biodiversity. By bias and background I may be prejudiced; I am therefore open to adaptation and criticism.

⁹ <http://www.human-evol.cam.ac.uk/duckworth.html>

The main question of this paper is concerned with the terms: endurance running, calcaneal morphology, energetics and predictive simulations. These are shortly elaborated upon here, but will be elaborated further upon in the **Background** and **Method** sections. Endurance running performance is often quantified using four major biomechanical and physiological demands on the body [1, 2]. These four demands are; energetics, stabilization, strength and thermoregulation. Related to energetics Larsen [3] stated three prerequisites for an athlete to be successful in endurance running. These three prerequisites are a high capacity for aerobic energy output (VO₂max), the ability to use it for long periods and a good running economy [3]. Running economy will be used in this paper to evaluate the effect of calcaneal morphology on endurance running performance. The running economy of an individual is the mass-specific metabolic energy cost of running at a given speed and is often evaluated by cost of transport in J/kg/m. In this paper running economy will be evaluated by using cost of transport values. Cost of transport is often expressed as oxygen consumption in moving a unit distance at a given speed normalized to weight, in this case cost of transport is measured on a performing athlete where oxygen consumption can be quantified. Since this paper will evaluate running economy from skeletal material, these measurements are not possible. To quantify endurance running performance using skeletal material, biomechanical models are required; these models use the current knowledge on kinetics and kinematics to simulate locomotion and phenomenological energy models can be used to quantify running economy. Physics based 3D predictive simulations of the musculoskeletal system allows for evaluating a wider range of hypotheses. The physical dimensions of the human body such as calcaneal geometry can be changed in these models. This allows the use of osteological measurements and the evaluation of its effect on endurance running performance without the use of experimental data. The running simulations performed in this study are at 4 m/s (14.4 km/h), an arbitrary intermediate endurance running speed. Besides cost of transport, the effect of varying tendon stiffness, speed (1.33 m/s) and settings are evaluated.

There are many biomechanical factors in the lower extremity that influence locomotive economy; many of these advantages find their origin in human evolution. Most of these factors are not only related to endurance running but also to walking. Current research mostly focuses on the time when humans became bipedal and only traits specific to walking are investigated, assuming that endurance running coevolved with walking. Some of the lower extremity musculoskeletal factors are summarized in table 1. These factors will not be discussed further since this paper focuses on a single trait specific to endurance running.

Trait	Effect	Benefits	Source
Reduced distal limb mass	Reduces energy cost	ER	[1]
Relative longer lower limbs	Reduces energy cost	ER and walking	[7, 8]
Plantar and transverse arch	Reduces energy cost	ER	[9, 10]
Short toes	Reduce energy cost	ER	[11]
Enlarged calcaneal tuber	Increases stability	ER and walking	[12]
Adducted hallux	Increase stability	ER and walking	[9, 10]
Lower extremity joint surface area	Increases stability	ER	[13]

Table 1: This table shows a summary for lower extremity characteristics that are attributed to enhanced walking or running performance. This table does not claim to represent a true or full overview, for a more extensive overview and upper extremity factors see table 1 in Bramble & Lieberman [1]. ER = Endurance Running.

One of the major biomechanical advantages specific to endurance running performance is related to the Achilles muscle tendon unit. The role of the Achilles on endurance running is studied intensively [14, 15], and it has been shown that running economy is strongly related to the properties of the Achilles tendon and its moment arm. The gastrocnemius and soleus muscles are the dominant plantarflexing calf muscles; these muscles form the triceps surae muscle group and attach to the calcaneum via the Achilles tendon. The muscle tendon unit acts on the ankle joint with a moment arm from the tendon to the ankle fulcrum (talocrural joint). The morphology of the calcaneum is a proxy for the effective moment arm of the Achilles with respect to the talocrural joint. As hypothesized by Raichlen [14] and Scholz [15], a shorter heel (i.e. smaller moment arm length) would be more energetically favorable. They base this hypothesis on the fact that the Achilles tendon functions as a non-linear spring with viscoelastic properties. The viscoelastic mass-spring properties of the Achilles tendon enable it to absorb and reutilize energy during running. During tendons stretch at heel strike energy is stored, during the subsequent toe-off this energy is reutilized in the muscle. The energy stored in the Achilles tendon is a function of tendon mechanical properties (tendon slack length and tendon stiffness), the forces that stretch the tendon and the moment arm of the tendon [14, 15]. It was found that mainly the length of the Achilles tendon moment arm was determining the energy stored in the tendon and a shorter moment arm leads to a greater stretching of the tendon and more conversion of kinetic energy to elastic energy. The skeletal correlate of the Achilles tendon moment arm is the calcaneal tuber length [14]. The calcaneal tuber length is the distance between the posterior edge of the calcaneal tuberosity and the anterior edge of the posterior talo-calcaneal surface. The study by Raichlen and colleagues showed strong correlation between Achilles moment arm and calcaneal tuber length ($r=0.95$; $p = 0.0002$). This measurement will be used to evaluate cost of transport using 3D predictive simulations under the assumption that increased elastic energy reutilization results in a better running economy.

2. Background

To understand the relationships between calcaneal tuber length, the Achilles muscle tendon unit and endurance running performance in evolutionary context, background information is provided. This background information is structured in two parts. Subchapter 2.1 describes the evolutionary history of human locomotion, considering specific selection pressures on bipedalism and endurance running. It will culminate in the specific evolutionary tale of the foot. Subchapter 2.2 is entirely focused on the biomechanics of human locomotion, describing the functional anatomy, and the principles of kinetics and kinematics. The background information is extensive as the intention is to make this paper accessible for all backgrounds.

2.1 History of human locomotion

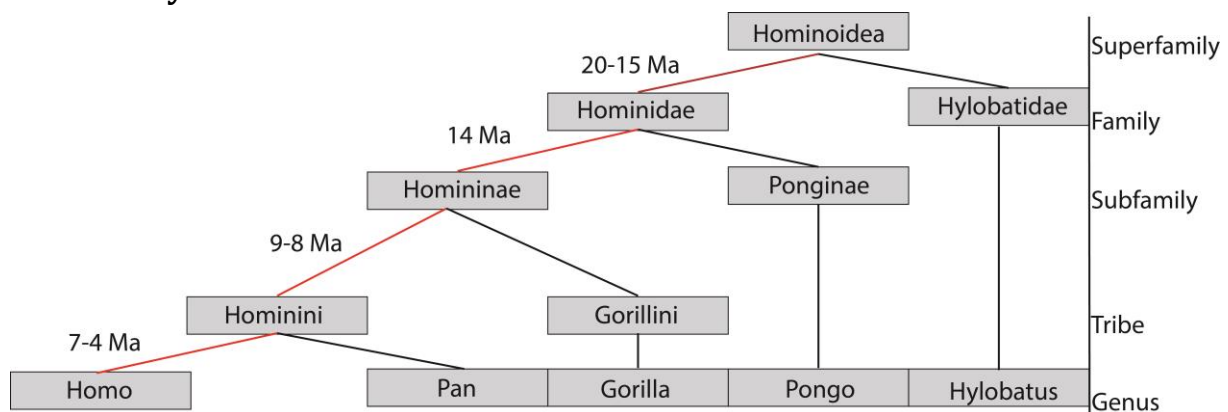


Figure 1: an evolutionary tree showing part of the Order Primates. It shows the relationship between the genus *Homo*, Great Apes (Orangutan, Gorilla, Chimpanzee and Bonobo) and Lesser Apes (Hylobatidae). The red line shows the direct lineage towards the modern *Homo sapiens*.

Subchapter 2.1 describes the origin of bipedalism and the transition from walking to running. It reviews the standing hypotheses concerning the selection pressures and subsequent morphologic adaptations for endurance running. Primates diverged from other mammals somewhere during the Late Cretaceous, but first fossil evidence stems from the Early Eocene [5]. *Homo sapiens* belong to the Order Primates, a hominoid group that diverged from the Old World Monkeys. The order Primates encompasses all ancestral apes and their descendants (see figure 1). The tribe Hominini diverged from the Gorillini (Gorillas) tribe around 8 million years ago and in turn the sub-tribe Hominina diverged from the Panina (Chimpanzees) around 5 million years ago.

This paper is considered with the part of human evolution when the divergence between chimpanzees and an ancestral hominid was completed and picks up the story where early hominins started to abandon their arboreal niche. The cradle for human evolution is situated in East Africa. Here, early hominins abandoned the arboreal niche and began to adapt to a more terrestrial niche. Several questions arise from this transition, and plentiful literature on this matter exists [6]. When and why did early hominins abandon the arboreal niche and began to adapt to bipedal locomotion? And how is bipedal walking related to the emergence of endurance running? These questions will be reviewed in the following sections.

The origin of bipedal walking and running

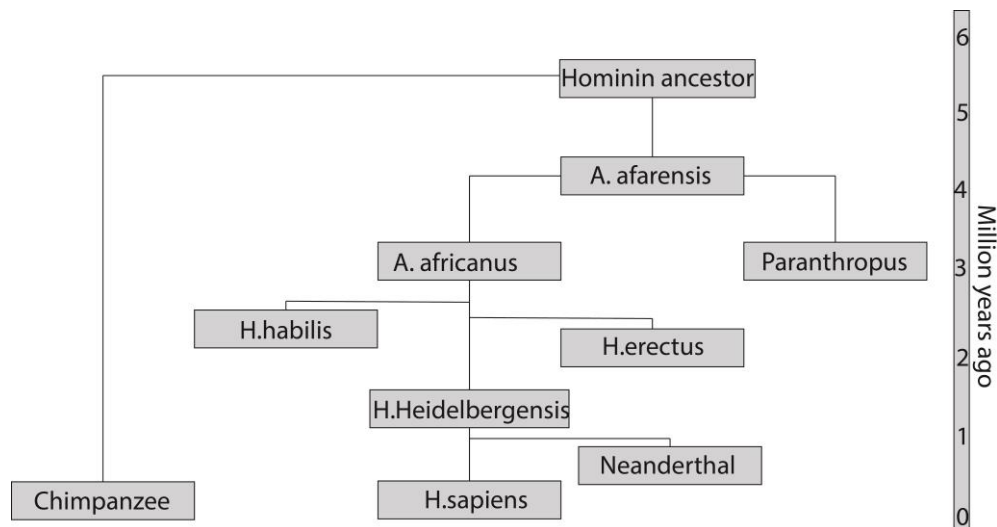


Figure 2: continuation of figure 1 showing the lineage from the hominin ancestor to *Homo sapiens*. The genus *Homo* emerged around 2.2 million years ago, about two million years after the emergence of the first hominin genus *Australopithecines*. The phylogenetic relationship between hominins is still a debated topic, and therefore this phylogenetic tree is not aimed to represent factual relationships, but a mere comparison.

Human bipedalism evolved from a generalized arboreal ape ancestor [16] or a terrestrial knuckle walking ancestor [17] (figure 2). Studies have shown that human bipedal walking is about 75% less costly than both quadrupedal and bipedal walking in chimpanzees [18]. This finding supports a long standing hypothesis stating that the transition to bipedalism from a knuckle walking ancestor involved a reduction in the cost of locomotion. This hypothesis remains unproven due to insufficient evidence from the fossil record. Whichever the ancestor may have been, bipedal walking evolved quite rapidly after the divergence of chimpanzees and early hominins. Trackways and postcranial material from the hominin genus *Australopithecus* found in Tanzania and Ethiopia provided fossil evidence of bipedal walking at about 3.6 million years ago [19, 20]. Based on morphologic studies on the *Sahelanthropus tchadensis* it may have been 7 million years ago [21], or based on morphologic studies on the ape *Danuvius guggenmosi* it may even have been 12 million years ago [22]. The anatomical evidence in these papers is disputed, but if proven would place the appearance of bipedal walking directly after the divergence of early hominins from chimpanzees. No unambiguous fossil evidence on the emergence of endurance running exists. Trackways indicative for running or specific skeletal traits have not been found. Morphologic studies on *Australopithecus* and *Homo erectus* show that *Homo erectus* had evolved traits for endurance running not seen in *Australopithecus*. This would place the emergence of endurance running capabilities around 1.9 million years ago [1, 2, 6]. In literature the focus has always been on bipedal walking, and it has always been assumed that selection pressure for walking resulted in similar traits required for endurance running. However, based on the biomechanical differences between walking and running, endurance running is not merely a byproduct of bipedalism [1]. The mass-spring mechanics of running (see [Biomechanics of human locomotion](#)) is inherently different to the inverted pendulum mechanics of walking. The fact that modern humans have traits specifically related to endurance running is evidence for specific selection pressures for endurance running. The next section describes the selection pressures early hominins experienced from the Late Pliocene (*Australopithecus*) to the Early Pleistocene (*Homo erectus*) and seek answers as to why hominins developed the ability to walk and run.

Natural selection pressure for bipedal walking and running

The process of human evolution is shaped, guided, accelerated or slowed down by a large number of factors. These can be 'internal factors', i.e., they are only felt within a specific species. Examples are competition, disease and predation. Internal factors are considered to be biotic in nature. 'External factors' can also play a role in the evolution of species, mainly by influencing the species' habitat. An important external factor is climate change [23]. Human evolution must have been subjected to both these evolutionary factors.

The internal evolutionary natural selection pressures important for human evolution are competition and predation, these selection pressures lead to species adaptation or speciation. The individuals having advantageous traits concerning competition and predation pass on these traits and thereby contribute to establishing this trait. Three important complementary hypotheses exist relating competition and predation to human locomotive evolution. The first hypothesis compares the morphology of early hominins with modern humans and based on biomechanical inferences gives a valid explanation for early hominids abandoning the arboreal lifestyle and committing to bipedalism. The second and third hypotheses focus in detail on the role of persistence hunting and scavenging in the further development of specific traits. The external factors such as climate are related to these three hypotheses and will be discussed appropriately.

The first hypothesis relates the tradeoff between intraspecific fighting and locomotion capabilities within early hominins to the development of bipedalism. It states that both locomotion and fighting are critical to survival and reproductive fitness in early human evolution, and that these two features are the main internal selection pressures determining adaptations in the postcranial morphology in early hominins [24]. In his paper David Carrier argues that morphologic features which make an individual good at fighting may in many cases limit locomotor function and vice versa. Based on morphologic evidence primates and early hominins show traits that would favor climbing and fighting capabilities over bipedal locomotive capabilities. According to this tradeoff these traits would limit the development of locomotive capabilities. The analogue between greyhound/pit-bull dog breed and *Homo sapiens/Australopithecus* was used by Carrier [24] to demonstrate this tradeoff. Basic biomechanical principles showed that pit-bulls have many traits that would favor fighting performance. Pit-bulls have more mass in their distal limbs, more muscle mass in their forelimbs compared with their back limbs and a shorter sturdier build. A greyhound has relatively long limbs, less muscle mass in these limbs and relatively more developed tendons. These traits would favor locomotive capabilities and limit fighting capabilities. These principles can be argued to exist between different hominin genera. Compared to *Homo sapiens*, *Australopithecus* had shorter legs, longer arms, and relatively more mass in the distal limbs. These features in combination with an increasingly more plantigrade posture are linked to the bipedal fighting behavior of great apes [25, 26]. Shorter legs would lower the center of mass and the plantigrade posture would increase the capacity to apply free moments to the ground, both advantageous for fighting. Sexual dimorphism is observed within *Australopithecus*, where males have more mass in the distal limbs. This shows that the forelimb specialization was specific for male-male fighting and not purely adaptations to the arboreal lifestyle. Since primates prefer to fight on the ground it was argued that selection for increased male-male fighting may have helped draw the ancestors of *Australopithecines* to the ground. Environmental stress (external selection pressure) on the habitat of the early hominins may have affected the pressure to find new habitats and to fight with other early hominids over new habitats. The subsequent invention of new primitive weapon technology by early hominins reduced

the internal fighting selection pressure and allowed for more independent evolutionary development of the fighting and locomotive characteristics. The independent evolution of locomotive capabilities relative to fighting capabilities may have resulted in a new predatory niche, the niche of the persistence hunter.

The second hypothesis is concerned with the persistence hunting strategy. This hypothesis was first formulated and studied in detail by David Carrier [19]. The persistence hunting strategy relies on physiological demands of running from both predator and prey. The persistence hunting strategy states that natural selection for endurance running performance led to the developments of specific running traits. These traits would allow hominins to outrun prey until exhaustion or to get close enough for the use of primitive weapons. Persistence hunting in the modern world is rarely observed [27], but from literature it is known that some ethnic groups in Africa and South America still apply this method. The Tarahumara Indians are known to chase deer through the mountains of Northern Mexico until the animals collapse from exhaustion [28], and the Kalahari Bushmen [29] are also known for the same persistence hunting techniques. Normally the predator prey relationship is described as a functional tradeoff between anaerobic and aerobic metabolism [30], where natural selection favors speed (anaerobic) over endurance (aerobic) capabilities. Humans however, are an exception to this, and according to the persistence hunting theory, endurance capabilities are the favorable natural selection force. The persistence hunting theory mainly relies on two of the four physiological demands described before, namely thermoregulation and energy [19]. Most mammals control their thermoregulation by evaporative cooling, which lowers and maintains the core body temperature. Evaporative cooling occurs by respiration and sweating. The effectiveness of this thermoregulatory system depends largely on ambient temperature; a higher ambient temperature is unfavorable for evaporative cooling as less heat can be transferred to the environment. The respiratory cycle of many mammals is linked to locomotion, where the effectiveness of breathing depends on the gait type chosen. For most mammals, this linkage often limits the effectiveness of panting while running and thus limits respiratory cooling. Humans have the ability to sweat and pant effectively during running and lack insulating hair cover, these traits result in the most efficient way of thermoregulation when compared with other mammals. Early hominins had better thermoregulatory efficiency than their prey, enabling them to keep chasing prey until exhaustion or overheating. The second demand concerned with the persistence hunting theory is energetics. It is known from cost of transport studies that energy expenditure during running is different in humans than most other mammals [1, 19]. Most mammals have different gaits such as walking, running, trotting and galloping. It is thought that humans select gait features such as step frequency and length that optimize their cost of transport [31]. Walking, trotting and galloping have an optimal cost of transport at a certain speed, a speed at which that gait is most energetically favorable (figure 3). The running gait of humans however does not have an optimal cost of transport at a certain speed, running a marathon at a slow pace results in the same energy expenditure as running a marathon at higher paces.

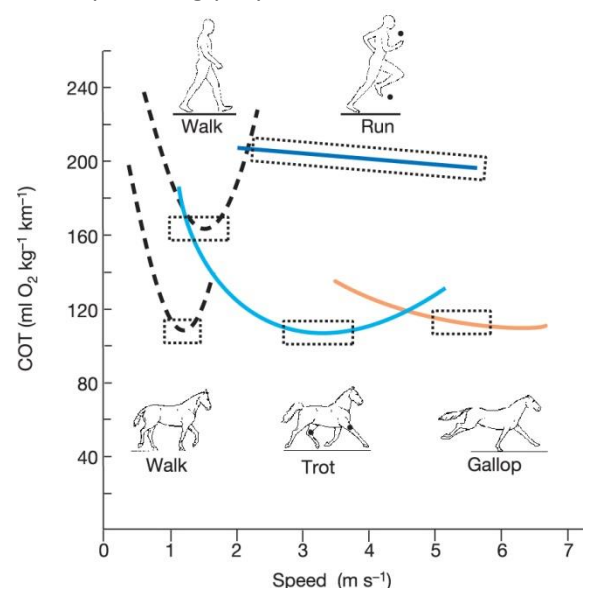


Figure 3: cost of transport comparison between human and horse. Running cost of transport for humans does not vary with speed, as opposed to most other mammals. Figure is from Bramble & Lieberman [1].

This markedly different feature arises from the human bipedal posture, which allows humans to vary breath frequency relative to stride frequency. Returning to the persistence hunting hypothesis, early hominid hunters had the option to choose a speed least economical for a certain prey type within their aerobic cost of transport range for running. This range would coincide with a maximum cost of transport for a certain prey, driving it to exhaustion rapidly. The persistence hunting theory is only valid for the period where hunting with advanced weapons did not exist. Advanced weapons such as the bow and tipped spears would be energetically favorable over persistence hunting. The Pliocene to Early Pleistocene is known for its primitive tools and weapons. These primitive tools were not primarily used for the hunt, but only for the final killing blow and the processing of the kill. The habitat is also essential for the validation of the persistence hunting; it is primarily suited to open habitats, such as savannas and (semi)deserts. The third hypothesis is related to the persistence hunting theory, but it involves scavenging rather than active hunting. The scavenging hypothesis states that selection for endurance running capabilities would lead to the development of similar running traits used for persistence running and enable early hominins to arrive at dead prey before other hominins or competing carnivores (first come, first serve). This theory does not rely on the thermoregulatory abilities of prey and predator and thus would be a more valid theory for non-arid habitats.

The evolution of the human foot

Since this paper is focused on the foot and the calcaneum and its relation to the Achilles tendon specific, the next section will review the current understanding about the evolution of the human foot. In the section “**Biomechanics of the ankle and foot**” the biomechanical aspect of the Achilles tendon will be explained.

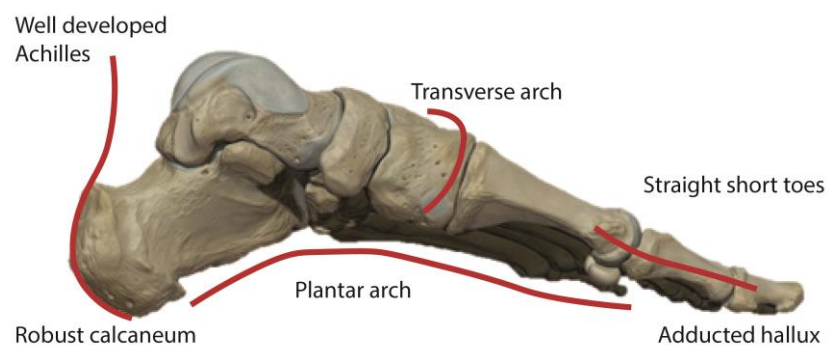


Figure 4: ankle and foot anatomy, showing the main features related to bipedal walking and running. These features are found to be well developed in fossil material starting at the genus Homo. A well-developed Achilles tendon in this context indicates a thicker, longer and more pronounced tendon than observed in extant apes. Figure used with permission from creator Catherine Sulzmann¹⁰.

Human plantigrade foot posture is a derived character of apes, the human foot aids in the support of the body weight [26], it functions as a propulsive lever and it acts as stress dissipater at heel strike. From the human foot morphology bipedalism can be inferred, important aspects are the presence of longitudinal and transversal arches, the robusticity pattern of the metatarsals, the adducted hallux and the established presence of the Achilles tendon (figure 4). All of these features are indicative for enhanced bipedalism and are not well-developed in apes. The Achilles tendon, the foot arches and the calcaneum morphology can also be attributed to enhanced endurance running capabilities. Foot

¹⁰ <https://sketchfab.com/csulzmann>

morphology is described in literature by Pablos [32] and Holowka and Lieberman [10]. From these papers it becomes evident that the amount of calcaneal fragments is limited. Holowka and Lieberman divide the general evolution of the foot in three stages. The first stage is concerned with *Ardipithecus ramidus*, the second stage concerns with early hominin *Australopithecus afarensis*, and the third stage is concerned with the early members of the genus *Homo*.

The first stage describes the locomotive capabilities of *Ardipithecus*, who belongs to the same sub-tribe as *Australopithecus*. Foot morphology shows relatively more adaptations to arboreality than to bipedalism. An opposable (non-adducted) hallux is present; an opposable hallux is associated with arboreal grasping and often indicates the absence of a developed longitudinal arch. The other phalanges were long and curved, also indicative for arboreality. However, some evidence described in the paper by Lovejoy 2009 [33] indicate the *Ardipithecus ramidus* was occasionally bipedal. The second stage is concerned with the genus *Australopithecus*. The locomotive capabilities of *Australopithecus afarensis* have been studied quite extensively [12, 34], and based on morphologic studies and fossil trackways it has been argued that *Australopithecus afarensis* was able to climb and walk albeit in differing efficiencies. The genus *Australopithecus* is believed to be an intermediate stage when considering the evolution of the foot to bipedal walking and running. *Australopithecus* had relative longer arms than legs indicative for arboreality. However, when considering the feet, *Australopithecus* shows more adaptations to bipedalism than *Ardipithecus ramidus*. The trackways of *Australopithecus* are characterized by deep heel impressions, a slightly abducted hallux and a shallow medial mid foot print. These indicate human like heel weight bearing and the presence of a longitudinal arch. Bramble and Lieberman [1] hypothesize that *Australopithecus* did not have a well-developed human-like tendon and estimate that modern-like Achilles tendon properties emerged around the appearance of the genus *Homo*. Three calcaneal fragments belonging to *Australopithecus* specimen from the Hadar site in Africa have been studied by Latimer [12] and Susman [34], the material from Hadar has been dated to be 3.2 million years old. The three studied Hadar calcanei showed a small lateral plantar tubercle [12, 34] (see figure 8) when compared with modern humans. A large lateral plantar tubercle and an increase in overall bone volume aids in dissipating the load stress experienced at heel strike. Modern humans and early members of the genus *Homo* show a well-developed lateral plantar tubercle, as opposed to the *Australopithecus* from Hadar and extant apes. The prominence of the lateral tubercle in modern humans is related to the orientation of the talocrural axis. A more obliquely orientated axis (coronal plane) observed in apes creates more supination at dorsiflexion and results in supinated heel strike. Humans and early hominins show a more horizontal talocrural axis resulting in a less supinated dorsiflexion and more lateral stress at heel strike, to account for this increased lateral stress, the lateral tubercle became more expressed. Another aspect which differs between hominins and apes is the long axis convexity of the talar posterior articular surface. This joint convexity will reduce as a direct correlate of increasing body size or loading. Hadar specimen showed a relative reduced convexity of this joint axis compared to African apes, therefore implying it could withstand the higher loads accompanied by bipedal walking. Joint articular surfaces of the tarsal and metatarsal fossils indicate the presence of both the longitudinal and transverse arches. Based on these anatomical findings of the Hadar postcranial material, Latimer and Susman claim that *Australopithecus* was insignificantly arboreal around 3 million years ago. Specimens of *Australopithecus sediba* were found in South Africa, dated to be 1.98 million years old and including an intact calcaneum [35]. The morphology of this bone showed a rather primitive configuration compared with the *Australopithecus* specimen from Hadar and Homo

sapiens. It lacked the eminence of the lateral plantar tubercle and had a relative slender calcaneal tuber. It did however show evidence for a humanlike tendon insertion for the gastrocnemius and soleus muscles. The rest of the skeletal material from *Australopithecus sediba* was comparatively more similar to humans than to apes. The fact that the older calcaneal material from *Australopithecus afarensis* from Hadar was evidently more modern-like in terms of endurance running than the *Australopithecus sediba* demonstrates the complexity of bipedal evolution and the lack of sufficient fossil data. The third stage is concerned with early species of the genus *Homo*. Foot bones from *Homo habilis* and *Homo erectus* show further development towards human like locomotion. A 1.8 million year old foot from Tanzania attributed to *Homo habilis* shows evidence for a fully adducted hallux and modern human like midfoot joints [36]. Fossil feet bones attributed to *Homo erectus* from a 1.8 million year old site in Georgia also provide evidence of a fully adducted hallux [37]. Footprints from multiple individuals belonging to *Homo erectus* have been found in Kenya, these footprints were dated to be 1.5 million years old [38]. The footprints show evidence for human like weight transfer, where weight transfer occurs from lateral hind foot landing to medial fore foot toe-off. They also found relative shallow footprint depths near the medial mid foot, which is evidence for a well-developed longitudinal arch. The trackways were attributed to males, and it is believed that it consisted of a male-male cooperative group engaging in foraging activities.

Subchapter 2.1 can be summarized as follows: the main internal drivers of human locomotive evolution are 1) independent evolution of fighting and locomotive capabilities 2) increased selection pressure for persistence hunting capabilities and 3) increased selection pressure for scavenging capabilities. A common ancestor of the early hominin left the arboreal lifestyle to gradually become committed bipedal and develop running capabilities. The common ancestor may have been drawn to the ground due to intraspecific selection pressures such as male-male competition and/or habitat changes. The terrestrial realm, being a new niche, represented new opportunities for feeding strategies. The persistence hunting and scavenging theory describe how the early hominin experienced selection pressure for endurance running performance. External factors resulting in selection pressure for bipedal walking and running have not been considered in detail. Climate change is the most likely external factor that influenced the habitat of early hominins and may have contributed to evolutionary change. The relationship between climate change and faunal evolution is elegantly described in a paper by Van Dam [39], where Milankovitch cycles are related to certain tipping points (i.e. speciation and extinction) in faunal evolution. It is believed that climate change related to for example Milankovitch cycles can be responsible for large scale changes in postcranial morphology. External factors will not be elaborated upon further, as that is not the primary scope of this paper. The internal selection pressures described explain the postcranial morphologic changes observed from ancestral hominins to modern humans. Fossil evidence agrees with the proposed selection pressures towards bipedal walking and running. The evolution of the feet demonstrates the adaptations to increased bipedalism and endurance running; the toes become shorter and the hallux becomes more adducted, these represent a change from arboreality to bipedal walking. The calcaneum becomes more robust for weight bearing, the transverse and plantar arches develop as energy saving mechanisms and the Achilles tendon is thought to become thicker and longer in conjunction with the development of these arches to contribute to these energy saving mechanisms.

2.2 Biomechanics of human locomotion

From the perspective of human evolution, it is now evident that certain morphologic traits emerged due to natural selection pressure towards endurance running capabilities. In this section the background information on human evolution will be linked to the current understanding of biomechanics. The field of biomechanics is focused on understanding the neuromusculoskeletal system related to the kinetics and kinematics of motion. This section will describe the functional anatomy, describe the mechanics of walking and running and zoom in on the mechanics of the foot and ankle. All of the biomechanical background information is in the context of the used model, which will be elaborated further upon in the [methods](#) section.

Functional anatomy

Running encompasses flexion and extension, abduction and adduction and rotational movements in the entire body caused by muscle tendon dynamics. These muscle tendon dynamics create joint torques which produces motion. The lower extremity joints important for running are the hip, knee, ankle and foot joints. The OpenSim musculoskeletal model used in this study models the lower extremity muscles and joints, the arms are driven by torque actuators. Therefore, a description of upper body musculature will not be given. In the following section the lower extremity musculoskeletal components of the used model and its functioning will be described (as in Hamill & Knutzen [40]).

The pelvis girdle and hip joint compose the most superior system of the lower extremity. The pelvic girdle is an attachment place for 28 muscles. In the model 19 different muscles are used to accomplish movement at the hip joint (see table 2). The hip joint is a ball-and-socket joint with 3 degrees of freedom (abduction-adduction, flexion-extension, rotation). Hip flexion mainly occurs by the iliopsoas muscle group and the rectus femoris, the strongest hip flexor is the iliopsoas muscle group. The rectus femoris muscle is a two-joint muscle (hip and knee) and its functioning depends on joint position. Secondary flexors of the hip are the sartorius, pectineus and tensor fascia latae. Hip extension occurs by the hamstring muscle group (semimembranosus, semitendinosus and biceps femoris longus) and the gluteus muscle group (maximus, medius and minimus). The hamstrings are the main hip extension muscles. The hamstrings also cross the knee joint and therefore their functioning as hip extensor depends on joint position. The main hip abductor is the gluteus medius, secondary abductors are the gluteus maximus, gluteus minimus, the piriformes, the sartorius and the tensor fascia latae. The adductor muscles are the gracilis, the pectineus and the adductor longus, adductor brevis and adductor magnus. Secondary adductors are the biceps femoris longus, the semitendinosus and the semimembranosus.

The knee joint has three articulating surfaces, the tibio-femoral joint, the patello-femoral joint and the tibio-fibular joint. The knee joint used in the model is as a custom joint and only allows knee flexion and knee extension, the knee joint is acted upon by 13 muscles in the model. The quadriceps femoris muscle group is the strongest knee extensor muscle. The muscle group consists out of the rectus femoris, vastus intermedius, vastus lateralis, and vastus medialis. The rectus femoris is the only muscle of this group that runs across both the hip and knee joint, and therefore its functioning as knee extensor depends on positioning of both joints. The most important knee flexor is the hamstrings muscle group, consisting of the biceps femoris longus, semimembranosus and semitendinosus. Secondary knee flexors are the gracilis, the lateral and medial gastrocnemius and the sartorius muscles.

The ankle and foot consist out of 26 bones and more than 20 muscles. The foot contains three major synovial joints, the talocrural, subtalar and midtarsal joints. In the model the ankle is a 2 degree of freedom joint, where 12 different muscles act on the ankle and foot joint to produce plantarflexion, dorsiflexion, eversion and inversion. The dominant plantarflexion muscles are the lateral and medial gastrocnemius and the soleus muscles. Secondary plantarflexion muscles are the peroneus brevis, peroneus longus, tibialis posterior and the flexor digitorum and flexor hallucis muscles. Since the gastrocnemius also crosses the knee its effectiveness depends on relative positioning of the joints. The most important dorsiflexion muscle is the tibialis anterior, aiding this muscle are the extensor digitorum, the extensor hallucis and the peroneus tertius.

Muscle	Joint	Action
Gluteus maximus	Hip	Abduction, extension
Gluteus medius	Hip	Abduction, external, rotation, internal rotation, extension
Gluteus minimus	Hip	Abduction, external rotation, internal rotation, extension
Piriformes	Hip	Abduction, external rotation
Sartorius	Hip	Abduction, flexion
	Knee	Flexion
Tensor Fasciae Latae	Hip	Abduction, flexion, internal rotation
Adductor magnus	Hip	Adduction, extension
Adductor brevis	Hip	Flexion, adduction
Adductor longus	Hip	Flexion, extension, adduction
Gracilis	Hip	Flexion, adduction
	Knee	Flexion
Iliacus	Hip	Flexion, internal rotation
Pectineus	Hip	Flexion, adduction
Psoas	Hip	Flexion, internal rotation
Rectus femoris	Hip	Flexion
	Knee	Extension
Gemellus	Hip	External rotation
Quadratus femoris	Hip	External rotation
Biceps femoris long	Hip	Extension, adduction
	Knee	Flexion
Semimembranosus	Hip	Extension, adduction
	Knee	Flexion
Semitendinosus	Hip	Extension, adduction
	Knee	Flexion
Biceps femoris short	Knee	Flexion
Lateral gastrocnemius	Knee	Flexion
	Ankle	Plantarflexion
Medial gastrocnemius	Knee	Flexion
	Ankle	Plantarflexion
Soleus	Ankle	Plantarflexion
Vastus medialis	Knee	Extension
Vastus intermedius	Knee	Extension
Vastus lateralis	Knee	Extension
Flexor digitorum	Ankle	Plantarflexion, inversion
Flexor hallucis	Ankle	Plantarflexion, inversion
Tibialis anterior	Ankle	Dorsiflexion, inversion
Tibialis posterior	Ankle	Plantarflexion, inversion
Extensor digitorum	Ankle	Dorsiflexion, eversion
Extensor hallucis	Ankle	Dorsiflexion, inversion
Peroneus tertius	Ankle	Dorsiflexion, eversion
Peroneus longus	Ankle	Plantarflexion
Peroneus brevis	Ankle	Plantarflexion, eversion

Table 2: an overview is provided of the muscles used in the model, including the joints they act upon and the respective motions they produce.

Biomechanical description of locomotion

In this section, a biomechanical analysis of human locomotion will follow. Biomechanical analysis of human locomotion is traditionally subdivided in kinematics and kinetics; kinematics deals with the spatial and temporal components of locomotion without considering forces, a kinematic analysis involves the description of a gait cycle to determine position, velocity and acceleration of the total body and its segments. Kinetics deals with the forces describing the kinematics observed. In principle both the walking and running gait cycles can be described using the same terminology and the same muscles, however, the two gait cycles do differ in certain aspects. The kinematics and kinetics will be described in the context of the walking and running gait cycles, both addressing their similarities and differences.

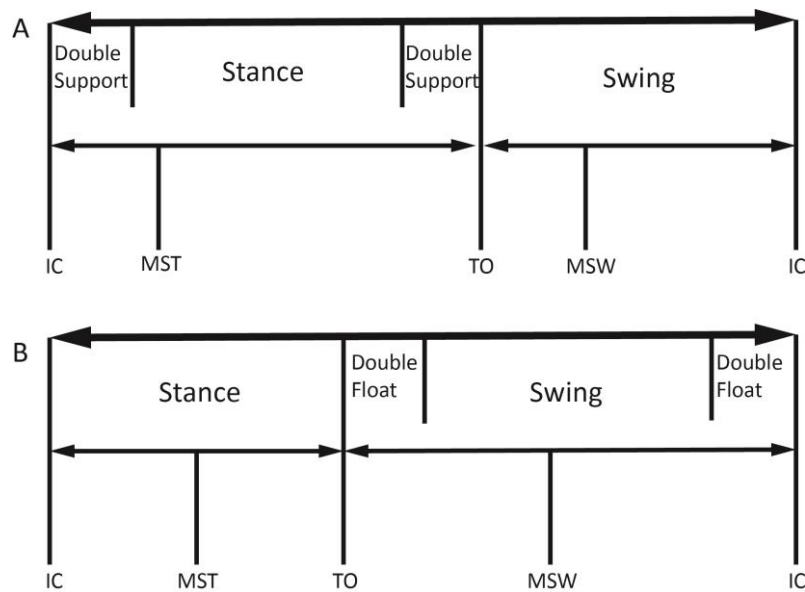


Figure 5: The walking (A) and running (B) gait cycles (Dugan & Bhat 2005 [41]). IC=Initial Contact, MST=Mid Stance, TO=Toe-Off, MSW=Mid Swing, IC=Initial contact. The main differences between walking and running are the percentage of the gait cycle spent in the stance phase, and the double support versus double float phases (see text).

Qualitative kinematic data can be obtained in various ways; the most common way is by using marker sets from experimental gait data. A gait cycle is the base unit of measurement in biomechanical analysis, it is defined as the time period between initial foot ground contact and repeated foot ground contact with the same foot (figure 5). During a gait cycle, the body components move through various positions in a predefined coordinate system and the marker sets record these movements. When marker sets are used, the position, velocity and acceleration of these components can for example be used as input for the model. The running and walking gait cycles are divided in the stance phase and the swing phase. The stance phase is subdivided in the heel strike, mid stance, heel-off and toe-off. The swing phase is subdivided in the mid-swing and the terminal swing phase. Increasing the speed of locomotion results in less ground contact time; for the running gait, toe-off occurs at 30 to 40% of gait cycle completion [43], for walking, toe-off occurs when at 50 to 60% of gait cycle completion. The transition from walking to running is also characterized by a change from the double support stance phase to a double float swing phase [42]. Double support indicates that both feet are in contact with the ground during the stance phase, double float indicates that both feet are not in contact with the ground during the swing phase. Walking can mechanically be described and modeled using an inverted pendulum model. The walking model describes the movement of the stance leg over the stance foot as inverted pendulum and the

swing leg like a regular pendulum about the hip. Potential and kinetic energy are out of phase and interchange under the absence of dissipative forces. Running can be described using a mass spring inverted pendulum model. As opposed to walking, the kinetic and potential energy are in phase; they both decrease in the absorption phase and increase in the propulsion phase. The energy however is not lost completely at absorption; much of the energy can be stored as elastic energy and reutilized in the subsequent propulsion phase. Therefore, running efficiency is more related to energy reutilization [42], than to the interchange of potential and kinetic energy, when compared with walking.

Both gait cycles are a continuous cycle of deceleration and acceleration, also called absorption and propulsion respectively. Absorption occurs during the first half of the support phase (heel strike and mid-support) and during the last part of the swing phase. During propulsion the center of mass moves forward and upwards, propulsion occurs at heel-off and toe-off at the end of the stance phase. Maximum forward propulsion occurs at the end of toe-off, this is also when energy stored in the tendon is reutilized. Heel strike is the first stage of any gait cycle; just before heel strike hip and knee extension occurs to prepare for impact. Then, at heel strike knee flexion and hip flexion occur and the foot is in a slightly dorsiflexed position. The downward movement of the body is also controlled by the eccentric contraction of the knee extensors. When the center of mass moves over the stance leg, the braking phase transitions into the midsupport phase, during the midsupport phase hip extension and knee extension occur. Hip extension by the hamstrings is important in supporting body weight during the midsupport phase; it assists in propelling the body up and forward. Knee extension is mainly controlled by the quadriceps femoris muscle group. During midsupport muscle activity is low in the lower leg, the dorsiflexing foot slowly transitions into a plantarflexing foot and body weight is centered above the leg. The foot is pronating from initial contact to midsupport and transitions towards supination at heel-off and toe-off. The toe-off phase is the main part of the stance phase propulsion. The rectus femoris contributes to the extension at the knee in the toe-off phase at the same time extension at the hip occurs. The quadriceps femoris produce the vertical velocity during the propulsion moment of the support phase. During the toe-off phase plantarflexion is used to propel the body forward and upward. Plantarflexion increases after heel strike and dominates through the stance phase. Plantarflexing muscles combined with the hip and knee extensors are the most important muscles for forward propulsion. When the foot leaves the ground the initial swing phase starts. At the hip, flexion occurs as the thigh is moved forward and upward. Hip flexion occurs by the iliopsoas and rectus femoris. Dorsiflexion at the ankle is actively used in the swing phase of running and prior to foot landing, as it controls the foot going down to the ground when landing. The hamstrings and hip extensors extend the hip around the mid swing phase prior to the next absorption phase. At the end of the swing phase the gluteus maximus and the hamstrings become active; the gluteus maximus and the hamstrings control the flexion of the trunk and decelerate the swing leg. The quadriceps muscle group is also active during the late swing until the heel strike to prepare for ground contact. When heel strike occurs again, one full gait cycle is completed.

Muscles produce motion by generating muscle force, the forces are produced by muscle tendon units under the control of muscle excitations. Muscle tendon units can be described using the Hill muscle model [43]. The forces result in the displacements of individual segments and in combination with external forces the overall displacement of the center of mass. The kinetics of the model can be described by the 1) muscle dynamics (contraction and activation), and 2) skeletal dynamics. Body segmental dynamics provide the information about how the model is built up. It provides information about all the segments, such as mass center, length and mass of the segment, and moment of inertia. It also provides information about the total number of muscles used, their relative origin and insertion sites, respective joints and degrees of freedom. Muscle dynamics describes both the activation and contraction dynamics. The Hill's muscle model (figure 7) forms the basic cornerstone to describe the muscle dynamics by identifying the active contractile component (CC) and two non-linear spring elements, the parallel elastic component (PEC) and the series elastic component (SEC). The contractile component forms the active force generating part of the muscle, which is the crossbridge formation in the muscle fibers. Cross bridge formation describes the mechanism for muscle contraction, where myosin and actin from an attachment detachment cycle in order to contract the muscle (see figure 6). The elasticity inherent in the muscle is represented by the SEC and PEC, with the PEC representing elasticity surrounding the muscle fibers and the SEC representing the tendon. Tendons can be seen as springs, with the muscles being the tensioners.

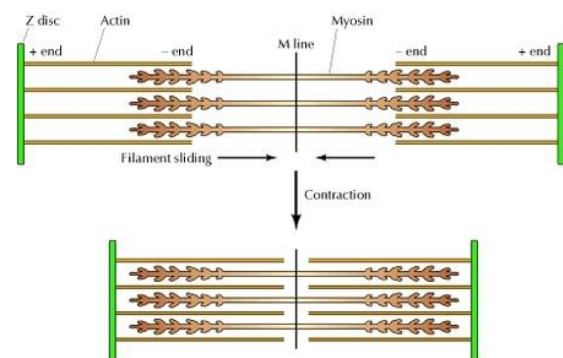


Figure 6: cross bridge formation in the contractile component of muscles. Actin and myosin proteins attach, pull and reattach in a cyclic manner during contraction. Figure source: *Structural Biochemistry: Actin and Myosin*.

The Hill type muscle tendon unit consists of a tendon with length L_t in series with a muscle with length L_m , the pennation angle α determines the angle between the tendon and the muscle fibers. Five parameters scale the generic properties of a Hill type muscle tendon unit to specific muscles, these properties are: maximal isometric force; optimal fiber length; tendon slack length; optimal pennation angles and maximal contraction velocity.

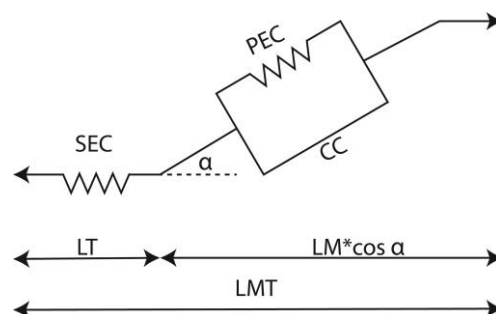


Figure 7: Hill's muscle model, describing the muscle and tendon using three components. Two elastic components are the series elastic (SEC) and the parallel elastic (PEC) components, the force generating component is the contractile component (CC). The muscle force generated is a function of activation, normalized length of the muscle unit (L_T , L_M and L_{MT}) and the normalized velocity of the muscle unit.

The activation dynamics describes how muscle excitations from the nervous system lead to muscle activation. It relates the time rate of change of muscle activation to muscle excitation, with corresponding rise and decay constants of muscle activation [44, 45]. The contraction dynamics describes the relationship between activation dynamics and force production. The static muscle tendon parameters influence the force-velocity-length relationship and elastic properties of the muscle tendon unit. The force-length relationship has an 'active' and 'passive' force domain. Optimum muscle force is produced at an optimum muscle length (\pm resting length). Active force generation decreases when the muscle is not at its optimum length, since cross bridge formation becomes less efficient, this relationship can be described by a Gaussian curve [44, 46]. Passive force generation in muscle fibers is related to the tissue surrounding muscle fibers, characteristics of this tissue are responsible for the passive muscle response when muscle fibers are stretched. Passive force generation increases when the muscle is stretched past its optimal fiber length and it can be described by an exponential function. Together these two curves describe the total muscle force-length relationship, where force initially increases as fiber length approaches optimal fiber length (active), levels off at optimal fiber length and then increases when fiber length becomes larger than optimal fiber length (passive). Active and passive force generation, in combination with the force velocity relationship, is part of the CC and PEC in Hill's muscle model [47]. The force-velocity relationship describes how the velocity of crossbridge formation is related to muscle force and activation. The amount of force generated by a muscle depends on the amount of crossbridges formed. It takes a finite amount of time for crossbridges to form, therefore increasing the velocity of muscle contraction results in less crossbridge formations and decreased force generation. The force velocity relationship can be described by a double hyperbolic curve. The last part important for formulation of the contraction dynamics is the series elastic component, which represents a tendon. Tendons are viscoelastic properties reacting nonlinear to force, they can store elastic potential energy when they are stretched by an external force. The stress strain curve of the SEC initially increases exponentially and linearly thereafter. Passive joint moments are often incorporated in models to remain within physiological range-of-motion limits; they represent ligaments and joint capsules. The muscle dynamics described above are summarized in biomechanical models using two differential equations (activation and contraction), that relate muscle excitation to muscle activation and the force-length-velocity relationship [48] (see [Methods](#)).

Excitations lead to muscle activations which in turn result in muscle contraction, when muscles contract, chemical energy is converted to mechanical energy and heat. The first law of thermodynamics states that the total amount of metabolic energy consumed is equal to the sum of the rate of heat liberated and the rate of work done [49, 50]. During muscular contraction heat is liberated, and if there is a change in muscle length, mechanical work is done. In muscles the total energy consumption can be partitioned into those that describe the heat liberated and into those that describe the work done. The quantification of metabolic cost in simulations often relies on the muscle dynamics used in the simulations themselves (e.g. Hill muscle model describing contraction and activation dynamics). The partitioning of energy liberation differs in literature; two phenomenological models of skeletal muscle energy expenditure are used in this paper. Umberger 2003/2010 [51, 52] developed a phenomenological model of skeletal muscle energy expenditure for use with a Hill-type muscle tendon model. This model states that the total energy expenditure is represented by four terms: the activation heat rate, the maintenance heat rate, the shortening/lengthening heat rate and the mechanical work rate of the CC. The model from 2003 was

updated to the model from 2010, differing mainly in how muscular energy is treated during muscle lengthening. Bhargava 2004 [50] also developed a phenomenological model for muscle energy consumption to be used in conjunction with the Hill muscle tendon model. In this model the total rate of muscular energy consumption is described as the sum of five terms: activation heat rate, maintenance heat rate, shortening heat rate, basal heat rate, and the mechanical work done. The two models show similarities in their terms, the first common aspect of both models is the activation and maintenance heat rate. The activation heat is tension-independent heat liberated when muscles are stimulated [50], energy is required for muscle activation and to maintain a certain level of activation. The amount of energy required for this aspect is linearly related to the amount of fast and slow twitch fibers. The maintenance heat rate is the stable heat rate produced during isometric tetanus contraction; it is also dependent on the amount of slow and fast twitch fibers. The second common aspect of both models is the shortening (and lengthening heat) rate of muscles, it describes the rate at which heat is produced during an isotonic contraction in excess of the heat liberated during an isometric contraction at the same force [50]. Different muscle fiber types result in different shortening and lengthening heat rate; fast twitch fibers have a greater heat rate than slow twitch fibers [51]. The third common aspect is the mechanical work rate, the mechanical work of locomotion is divided in two components; the work required accelerating or decelerating the center of mass during each step (external) and the work required to swing the limbs relative to the center of mass (internal) [24, 53]. Positive internal mechanical work occurs by concentric muscle contraction, where muscle shortening results in the (angular) displacement of the segment is in the direction of the muscle force. Eccentric muscle contraction results in negative mechanical work and the degradation mechanical energy to heat or conversion to elastic energy. External work is work done by the environment on the body. Two dominant external forces are the ground reaction force, where a force is exerted by the ground on the body and the gravitational force. The position and acceleration of the center of mass determines the direction and magnitude of the ground reaction force [42]. The forward trunk leaning in combination with the ground reaction force produced during plantarflexion produces forward acceleration. Both internal and external work can be related to muscle functioning, thus the mechanical work rate is the mass specific work rate of a muscle. Both models implement the same but formulate it differently. Muscle energy consumption occurs mostly during the stance phase and the step to step transition [54, 55] where muscle activity is highest, and it is relative low during the swing phase. Humans choose speed, stride rate and stride length, step width and vertical movement of the center of mass to minimize energy expenditure, these characteristics change when transitioning from walking to running, thus affecting the characteristics of muscle energy consumption. The two energy models will be used to compute cost of transport values of the respective models at both running and walking speed (see [Methods](#)).

Biomechanics of the human foot

The foot is a key component from which bipedal walking and running can be deduced. Traits such as the longitudinal arch, transverse arch, adducted hallux and the robustness of the bones have been mentioned. One trait related to endurance running is the Achilles tendon and its relation to the calcaneum. The calcaneum is the largest of the 26 foot bones and forms the attachment point for the Achilles tendon. The calcaneum has 4 articular joint surfaces, 3 interact with the superior talar and 1 with the distal cuboid. These articular joint surfaces are visualized in figure 8, including important anatomical landmarks. The articulation between the calcaneum and the talar is the subtalar joint. The articulation between the talar, fibula and tibia is the talocrural joint. The intrinsic foot muscles that attach to the calcaneum are the triceps surae, comprising of the gastrocnemius lateralis, gastrocnemius medialis and soleus muscles. Intrinsic muscles that origin from the calcaneum are the extensor digitorum, extensor hallucis and flexor digitorum. According to the Hill muscle model the triceps surae comprises of three parts. The first part is the contractile component, formed by mainly the soleus and gastrocnemius muscles, the second part is the passive elastic component formed by the inherent elasticity in the muscles, and the third part is the series elastic component formed by the Achilles tendon. The Achilles tendon is the strongest and thickest tendon in the human body [56], it has an average slack length of 15 cm and ranges from 11 to 26 cm. It begins near the middle of the calf being connected to the gastrocnemius and soleus muscles proximally and to the calcaneum distally. The tendon, being part of the SEC, has the capacity to store and recover elastic strain energy. The Achilles tendon exhibits properties similar to a spring [57], the spring shows viscoelastic properties, with a nonlinear stress-strain relationship. Normally the distance between the midpoint of the talocrural joint and the Achilles tendon comprises the moment arm of the Achilles MTU (figure 9). However, based on a study by Raichlen [14] the moment arm can also be approximated by the calcaneal tuber length, the length between the anterior part of the posterior talar articular surface and the attachment point of the calcaneum at the posterior side of the calcaneal tuber.

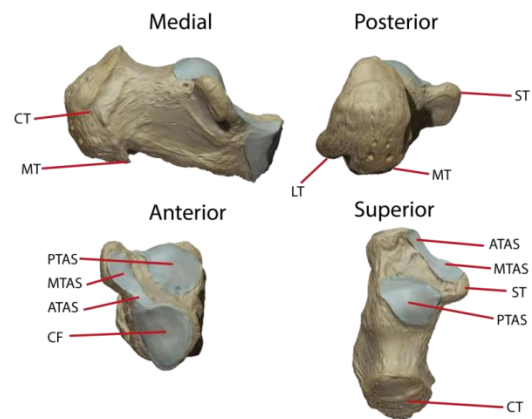


Figure 8: Morphology of the calcaneum in medial, posterior, anterior and superior views. CT = Calcaneal Tuber, MT = Medial Tuberosity, LT = Lateral/plantar Tuberosity, PTAS = Posterior Talar Articular Surface, MTAS = Middle Talar Articular Surface, ATAS = Anterior Talar Articular Surface, ST = Sustentaculum Tali. Figure used with permission from creator Catherine Sulzmann.



Figure 9: a simple first-class lever where the opposing forces are on opposite sides of the center of rotation. The joint moment (M_j) created at the ankle is the result of the forces by the gastrocnemius and soleus muscles (F_{mt}) and the moment arm (R). If the system is to remain in equilibrium (no acceleration) an opposing and equal force must be generated, this is the ground reaction force (GRF). In red is the moment arm between the talocrural joint and the tendon, in blue the moment arm between the anterior side of the posterior talar facet and the tendon (as in Raichlen [14]). Figure used with permission from creator Catherine Sulzmann.

During running, the contact time with the ground decreases and the tendon behaves like a spring. As in a spring, the amount of energy stored in a tendon is a direct function of its length, its elongation and the imposed force. A longer tendon slack length implies a greater capacity to store elastic strain energy [24]. The Achilles muscle tendon complex can be stretched up to 8% of its total length at heel strike [58]. The eccentric stretching of the Achilles tendon allows for energy absorption, this energy is released again when the muscles shorten concentrically to provide energy for plantarflexion [42]. All energy stored in a tendon does not need to be generated by the muscle and muscle specific energy consumption would thus decrease. However, the energy consumption of a muscle is also dependent on the amount of CC force generated, and CC muscle force is higher if the moment arm is smaller. Scholz [15] found that the variations observed in metabolic cost are associated more with generating CC work than force, thus implying that energy storage is more dominant than force production. The more force produced for a larger moment arm is relative insignificant when compared with the energy stored for a smaller moment arm. The amount of energy which can be stored in an element that is stretched over a distance under the influence of force is equal to the integral of the area under the tendon stress strain curve. The formulas below describe the relationship between energy (E), the muscle tendon force (F), joint moment (M_j) and the amount of strain (u).

$$F = ku^n \quad (1)$$

$$F = \frac{M_j}{r} \quad (2)$$

Formula 1 and 2 describe the basic way in how a muscle tendon unit can be modeled. The tendon force (F) is modeled as an elastic spring with u representing change in tendon length, k representing the spring constant and n is the order of the spring (linear, quadratic etc.). The magnitude of muscle tendon force (F) in turn is determined by the moment arm of the tendon (r) and the moment at the joint (M_j).

$$E = \frac{1}{n+1} * M_j^{\left(\frac{n+1}{n}\right)} r^{-\left(\frac{n+1}{n}\right)} k^{-\left(\frac{1}{n}\right)} \quad (n \neq 0) \quad (3)$$

The energy which can be stored in any material is the area under its stress strain curve. The integral of formula 1 (stress = F , strain = u) in combination with formula 2 results in formula 3 [15]. In biomechanics k is calculated based on maximal isometric force (F_{max}), the resting length of the SEC (Ise_0) and the elongation of the tendon at F_{max} (U_{max}). Based on this, Scholz defined the following formula for energy storage in a tendon.

$$E = \left(\frac{1}{n+1}\right) * M_j^{\left(\frac{n+1}{n}\right)} * r^{-\left(\frac{n+1}{n}\right)} * F_{max}^{-\left(\frac{1}{n}\right)} * Ise_0 * U_{max} \quad (4)$$

Function 4 provides support for the proposed hypothesis, for a given M_j : a smaller moment arm results in more energy stored in the tendon, and an increase in the tendon compliance increases the energy stored in the tendon. The formula also implies that for a given n , the energy stored in the tendon, is more sensitive to moment arm than to mechanical properties of the tendon. In the simulations metabolic energy expenditure can be evaluated by cost of transport (J/kg/m), total body energy expenditure (J) and muscle specific energy expenditure (J). The calculations are based on the two phenomenological energy models described before and not on equations 1-4.

3. Methods

3.1 Data collection

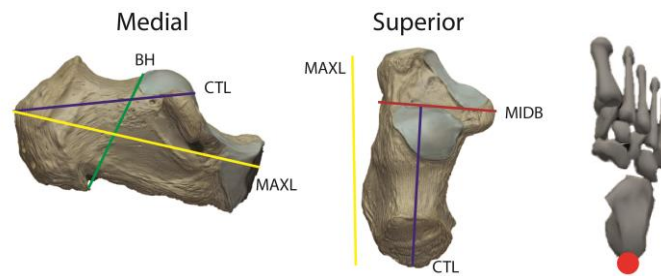


Figure 10: standard osteological measurements of the calcaneum in medial and superior views. BH = body height, MAXL= maximal length, MIDB = middle breadth, CTL = calcaneal tuber length. The calcaneum mesh in OpenSim with one virtual marker (red dot) is visualized on the right side. The scaling of the experimental data is performed based on placing the virtual markers accordingly. Figure used with permission from creator Catherine Sulzmann.

In total, calcaneal bones from 51 different subjects were measured. 29 calcaneal bones are from the Haya people of Kenya and 22 calcaneal bones are from the Saxon people of England. The Haya bones were recovered from a burial site near Lake Victoria, Kenya. The Saxon bones were recovered from burial sites in Sedgeford, England [59]. No accurate dating and sex estimation has been performed on any of the material, but both sample groups are within Holocene boundaries of age. Several standardized osteological measurements have been taken [60-63] (figure 10), these measurements were performed using standard electric sliding calipers. MAXL is the linear distance between the most anterior point of the calcaneus and the most posterior point on the calcaneal tuberosity. MIDB is the linear distance between the most lateral point on the calcaneus and the most posterior articular facet and the most medial point on the sustentaculum tali. BH is the linear distance between the superior and inferior surfaces of the body of the calcaneus taken in the coronal plane. CTL is the linear distance between the anterior part of the posterior talar articular surface and the most posterior point of the calcaneal tuberosity. CTL is representative for the moment arm between the Achilles tendon and the talocrural joint and is hypothesized to affect metabolic energy expenditure. The experimental measurements are used to scale the original model. The original model uses a predefined mesh with its own axial system to define calcaneal geometry. To use the experimental data in the model, the original calcaneal geometry needs to be rescaled in the x, y and z directions. This scaling was done in the OpenSim visualizer by placing virtual markers at geometric landmarks of the calcaneum (see figure 10). This provided three standard values for the x, y and z direction to which the experimental data could be scaled. The scaling was initially performed in three dimensions, using MAXL for the x-direction, BH for the y direction and MIDB for the z direction. The placement of markers is performed by visual identification of landmarks, which is subjective and prone to errors, but in relative terms this method of scaling still mimics the experimental data. First results showed that MAXL is highly correlated to CTL ($p=0.91$ for all data). For the scaling in the x-direction MAXL was chosen over CTL due to this high correlation coefficient and since scaling for MAXL proved to be more objective. First results also showed that scaling the calcaneum in 3 dimensions provided no correlation between MAXL and cost of transport ($r= -0.08$). To examine the effect of calcaneal length on the Achilles MTU and energy expenditure, the scaling to experimental data was then redone only in the x-direction. Six different models are created using the scaling tool; these correspond to the mean, maximal and minimal MAXL of both sample groups.

3.2 Predictive simulations

In the biomechanical background information, the following principles were mentioned; the relevant muscles and joints, the definition of the gait cycle, the subtle biomechanical differences between walking and running, the musculoskeletal dynamics, and the energy considerations. To perform 3D predictive simulations, these principles are essential. To perform 3D predictive simulations of movement a dynamical multibody system representing a musculoskeletal model is used. OpenSim is a freely available, user extensible software system that lets users develop biomechanical models of musculoskeletal systems and create dynamic simulations of movement. For a full overview of the functioning of OpenSim the reader is referred to the following papers [64-68]. In this paper the computational embodiment of OpenSim is combined with the formulation of an optimization problem in MATLAB. What follows in chapter 3.2 is 1) the relevant functioning of OpenSim and 2) the formulation of the optimization problem in MATLAB, in which the background information is implemented.

OpenSim is organized into computational and functional layers. The computational layer relies on the computational infrastructure Simbody. Simbody defines a computational system and state, and thereby classifies as state-determined system model. The system is the embodiment of all equations, respective bodies, joints and force elements required for a simulation. The state object can contain values that describe the variables used in the equations of a system; these include continuous time, position, velocity and other discrete variables. State determined system models require only the knowledge of its state variables at some initial time (t_0) and inputs for $t > t_0$ to determine the future behavior of the system. State variables evolve through time in a way that depends on the value they have at any given time and the imposed input variables, the output variables depend on the values of the state variables.

$$\dot{x}_n = f_n(x, u, t) \quad (5)$$

The differential equation (equation 5) above describes how each state (x) varies over time (t), under the influence of input u . For example, Joint angular displacements are state variables computed over time using differential equations, the joint angle at any time instance is the result of the current value of the joint angle and the input value. Input values can for example be muscle excitations. There are many of these equations describing the total system, these equations can be combined and used in matrix form to increase computational efficiency and reduce complexity. Each OpenSim models consist of several components with computational counterparts, these include bones (rigid bodies), joints (mobilizers, constraints and forces), contact elements (rigid constraints and compliant forces), and ligaments/muscle actuators (forces). OpenSim contains tools in the graphical user interface (GUI) that are part of the functional layer of OpenSim. Examples of these tools are; inverse kinematics, inverse dynamics, static optimization, and forward dynamics. These tools will not be used in this paper as they have certain limitations. OpenSim mainly provides tools for tracking problems, where kinetics and kinematics are both computed (inverse and forward) relying on experimental data. The objective of tracking simulations is to minimize the difference between the behavior of the model and experimental data [69]. When all components are combined to form a model, it will be able to stand with stiff joints or simply collapse. For simple simulative tasks the excitations and activations patterns can be assigned, for a whole musculoskeletal system this is too complex. OpenSim contains a tool for forward dynamic simulations called computed muscle control (CMC); it finds a set of muscle excitations that best match the kinematics and kinetics of experimental data.

Computed muscle control relies on experimental data and static optimization, both have their limitations in the accuracy of the forward simulation and the control the user has on the model. Computed muscle control relies on experimental kinematic data, calculating the kinetics (excitations) does not change the kinematics during the process. That is the major reason these tools are not used, changing the calcaneum morphology is expected not only to change the kinetics, but also the kinematics of the simulations. Using computed muscle control on measured kinematics would therefore be of limited realistic value. To overcome this problem, this paper uses predictive simulations. Predictive simulations do the opposite of inverse dynamics simulations: they generate *de novo* movements based on a mathematical description of the neuromusculoskeletal system without relying on experimental data. Predictive simulations have the potential to answer 'what-if' questions, this way the effect of changing the calcaneal geometry on the resulting motion can be observed. Until recently, predictive simulations have been hampered by high computational times due to the highly nonlinear muscle and skeleton dynamics [70]. Therefore, most studies have relied on conceptual models describing only the relevant part of the musculoskeletal system that sometimes exclude the activation dynamics. Such conceptual models are for example the simple pendulum model for walking and the spring loaded inverted pendulum model for running.

A computational efficient framework was established by Falisse and colleagues [71]. The framework is constructed in such a way that predictive simulations of gait can be formulated as an optimal control problem [69-71]. Solving an optimal control problem is a forward dynamics method; it tries to find and tune the important controlling factors (performance criterion) for a dynamical system (the musculoskeletal system) over a period of time (a gait cycle) such that an objective function (human gait) is optimized. If a ball were to be thrown from point A to point B, the ball can follow many different trajectories depending on the input variables. Optimization theory is used to describe how this trajectory would look like if it were to optimize the task with initial input, for example, minimize metabolic cost for the thrower. A major assumption is that such a trajectory is thought to be optimal in some sense. This is also believed for human motion, as can be explained by a simple observation: two people walking side by side never walk with the same stride length, stride frequency or speed. It is thought that both individuals walk the way they do because it minimizes (for example) energy consumption that is inherently connected to the different physiology of the two individuals. Optimization theory is built on this assumption [72], and currently it is thought that there are multiple controls governing human motion that can be optimized. In optimization the parameters that are optimized are called performance criteria, performance criteria for human motion are for example metabolic energy, muscle excitations or stride frequencies. In equation 5, 'u' can be thought of as the performance criterion, 'x' represents the system and its state variables and t represents time. 'x' and 'u' are vectors; the state variable vector 'x' comprises all state variables used. To optimize the objective function one could pick an arbitrary set of controlling factors and compute the state trajectory by forward integration. The resulting trajectory can be evaluated by the objective function value and subsequent multiple iterations then result in the optimal solution of the objective function. The optimal solution performs the task, while minimizing the performance criteria.

The computational efficient framework generates simulations in only 36 minutes on average in the study by Falisse [71], which is about 20 times faster than existing simulations with similarly complex models. This efficient computation is explained by the use of direct collocation, implicit differential equations and algorithmic differentiation. Direct collocation is used instead of direct shooting, this reduces the stiffness and nonlinearity problems encountered using direct shooting, thereby reducing computational time. The framework is formulated in MATLAB using CasADi and IPOPT software. MATLAB is used to set-up and solve the optimization problems, while OpenSim is used to represent the dynamic skeletal system. For a detailed description of the framework the reader is referred to the paper [71] and the corresponding code¹¹. An existing OpenSim musculoskeletal model was used with 29 d.f., 92 muscles actuating the lower limbs and trunk, eight ideal torque actuators at the arms and six contact spheres per foot was used [65, 68, 73]. Total body mass is 62 kg and is static for all simulations, the weight differences due to the scaling are negligible. Raasch’s model [45] is used to describe muscle excitation-activation coupling and a Hill-type muscle model [74] to describe muscle-tendon interaction and the dependence of muscle force on fiber length and velocity. Skeletal motion was modeled with Newtonian rigid body dynamics and compliant Hunt-Crossley foot-ground contacts [66]. The model used in this study relies on the muscle dynamical equations formulated by F. de Groot [74]. The redundancy problem (more muscles than joint constraints) is tackled by the formulation of the muscle dynamical equations as non-linear differential equations in combination with optimization theory. In the simulation the activation and contraction dynamics are also responsible for the coupling between time instants, thereby making it a dynamic rather than static optimization.

$$J = \frac{1}{d} \int_0^{t_f} \left(\underbrace{w_1 \|\dot{E}\|_2^2}_{\text{Metabolic energy rate}} + \underbrace{w_2 \|a\|_2^2}_{\text{Muscle activity}} + \underbrace{w_3 \|u_{dv,It}\|_2^2}_{\text{Joint accelerations}} + \underbrace{w_4 \|T_p\|_2^2}_{\text{Passive torques}} + \underbrace{w_5 \|e_{arms}\|_2^2}_{\text{Arm excitations}} \right) dt$$

The function above is from Falisse et al., 2019 [71], it describes the objective function (J) using certain performance criteria. Performance criteria that are minimized while describing the motor task are metabolic energy rate, muscle activity, joint accelerations, passive torques, and arm excitations. Most of these criteria are bounded by constraints to reduce the amount of outcomes (i.e. prevent unrealistic joint kinematics). The optimization problem also works with initial guesses; these reduce the complexity of the framework by limiting the amount of options for which the control problem can be tested. From experimental data on walking and running the limits of position, speed and accelerations of all individual segments can be known; the initial guess provides some insight to these limits and inhibits testing of unlikely solutions. The performance criteria generate trajectories of states by integrating system dynamical equations over half a gait cycle (assuming bilateral symmetry) in response to input controls and external forces. The performance criteria were assigned different weights until a cost function was found that produced human-like walking, this is the nominal cost function.

¹¹ <https://github.com/antoinefalisse/3dpredictsim>

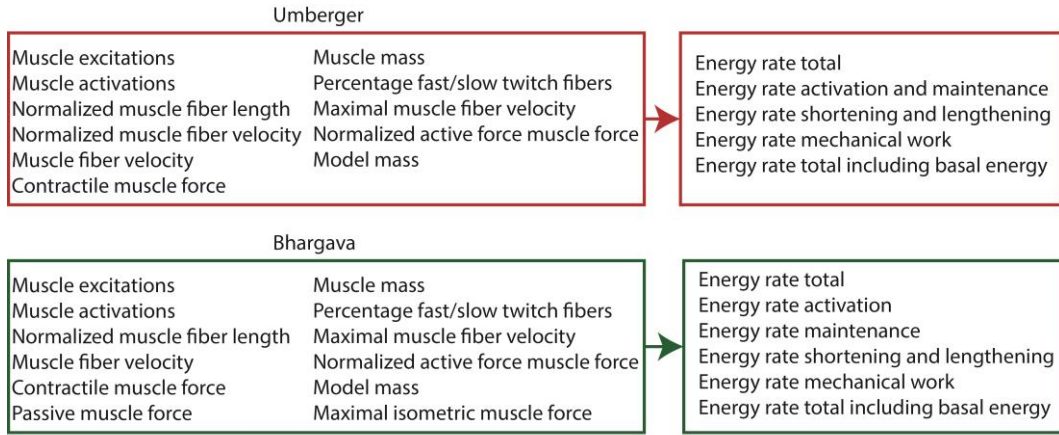


Figure 11: the inputs and outputs are shown for the two respective energy models. The Umberger model includes normalized muscle fiber velocity and excludes passive muscle force and maximal isometric muscle force with respect to the Bhargava model. The exact formulations of the equations and the output differ as well, as will be discussed in the discussion.

In this paper the nominal cost function is adapted, and the model is rescaled based on calcaneal measurements. Prior to the simulations, muscle tendon parameters (maximal isometric forces; optimal fiber lengths; tendon slack lengths; optimal pennation angles; maximal contraction velocities) are recalculated for the six models since scaling affects these properties. Muscle Analysis is then performed on all six models, this analysis gathers basic information about muscles during a simulation (e.g., forces, tendon lengths, moment arms, etc.). The muscle tendon data is then defined as a polynomial function of joint positions and joint accelerations. Polynomial functions are refitted after the Muscle Analysis. All simulations are performed at 4 m/s and 1.33 m/s. The framework established by Falisse has not been tested with speeds over 2.73 m/s, the boundaries and the initial guess of the system are adjusted in order to simulate at 4 m/s. The initial guess mode used is data informed, where a data informed guess for walking or running can be chosen. For the simulations performed at 4 m/s this initial guess is running, for the simulations performed at 1.33 m/s this initial guess is walking. The choice for the specific settings will be validated in the discussion. The effect of calcaneal tuber length on total body cost of transport (J/kg/m) is then evaluated. Two different phenomenological energy models used to calculate cost of transport are compared (see figure 11). Muscle specific energy consumption for the soleus, gastrocnemius lateralis, gastrocnemius medialis, tibialis posterior, flexor digitorum, flexor hallucis, tibialis anterior, peroneus brevis, peroneus longus, peroneus tertius, extensor digitorum and extensor hallucis is extracted. Tendon stiffness was adjusted for several simulations in order to evaluate the cost of transport sensitivity to tendon stiffness. The tendon stiffness of the soleus, gastrocnemius medialis and gastrocnemius lateralis was changed from 35 N/cm to 20 N/cm. The energy stored in the tendons of all aforementioned muscles is also evaluated. Energy stored in the tendon is calculated using the following formula:

$$E = FMo.* (lTr.* 5.0 - lTr.* shift.* 2.0e + 1).*(-1.0./2.0e + 1) + (FMo.* lTs.* exp(ATendon.* ((lTr + lTs)./lTs - 1.99e + 2./2.0e + 2)))./(ATendon.* 5.0)$$

FMo is the maximal isometric force a muscle can develop. lTr is the deviation of the tendon length with respect to the tendon slack length (lTs). ATendon specifies the tendon stiffness, which is by default 35 N/cm. Energy storage thus is a function of maximal isometric force, tendon stiffness and tendon length. These parameters coincide with the parameters seen in equation 4.

4. Results

Mean calcaneal tuber length of the Haya subjects is 54.94 ± 3.15 ; mean calcaneal tuber length of the Sedgeford subjects is 57.55 ± 5.41 . CTL size normalized to MAXL provides similar results, 0.713 and 0.716 for Haya mean and Sedgeford largest respectively. The main hypothesis states that the average calcaneal tuber length of the Haya subjects is smaller than the Sedgeford subjects. A one tailed Welch t-test ($\alpha=0.05$) was performed to evaluate average calcaneal tuber length differences between these two sample groups. A Welch t-test is an adaptation of the Student's t-test where unequal variance is assumed. The 29 Haya subjects as opposed to the 22 Sedgeford subjects demonstrated a statistically significant smaller average calcaneal tuber lengths, $t(32) = 1.69$, $p = 0.026$. This leads to the acceptance of the stated hypothesis. Scaling the calcaneum in 3 dimensions provided no correlation between MAXL and cost of transport ($r = -0.08$). The effect of scaling in the y and z directions is thought to obscure the effect of the scaling in the x direction. The simulations are thus performed only with models scaled in the x direction. Table 5 shows the results from the experimental osteological measurements. The Haya sample space ($N=29$) and the Sedgeford sample space ($N=22$) both resulted in three models, one showing the mean values of the entire sample space and 2 showing both the maximal MAXL and minimal MAXL. Prior to the simulations, the muscle tendon parameters are evaluated for each model. The muscle tendon parameters provide some basic input for the muscle tendon dynamic equations in the simulations. The results showed that, after scaling in the x-direction, the muscle tendon parameters differed between the models only for the following muscles: tibialis posterior, flexor digitorum, flexor hallucis, tibialis anterior, peroneus brevis, peroneus longus, peroneus tertius, extensor digitorum and extensor hallucis. Except for the tibialis anterior, peroneus tertius, extensor digitorum and extensor hallucis these are plantarflexing muscles (table 2). The muscle tendon parameters that were changed for these muscles are the tendon slack length, optimal fiber length and maximal contraction velocity. These showed a linear decrease from the Sedgeford largest to the Haya smallest model. Moment arm lengths did not change for the triceps surae, they did change for the muscles described above, and here too a linear decrease in moment arm length was observed from the Sedgeford largest to the Haya smallest model.

Model Name	MAXL	CTL	BH	MIDB
Haya largest (HL)	84.97	61.03	52.92	48.01
Haya mean (HM)	77.03	54.94	43.17	41.00
Haya smallest (HS)	65.67	49.01	36.10	36.33
Sedgeford largest (SL)	92.42	64.41	54.53	47.12
Sedgeford mean (SM)	80.37	57.55	47.97	41.285
Sedgeford smallest (SS)	69.62	48.34	43.67	36.19

Table 5: The table above describes 6 OpenSim models. Scaling in the x direction is done using MAXL, in the y-direction using BH and in the z-direction using MIDB. All values are reported in mm distance.

For the simulations performed at 4 m/s (subchapter 4.1) and 1.33 m/s (subchapter 4.2), the following is reported; 1) the relationship between cost of transport and MAXL, 2) the effect of different energy models on cost of transport, 3) muscle specific energy consumption per stride, 4) tendon energy storage per stride, and 5) the effect of varying Achilles tendon stiffness on cost of transport.

4.1 Endurance running

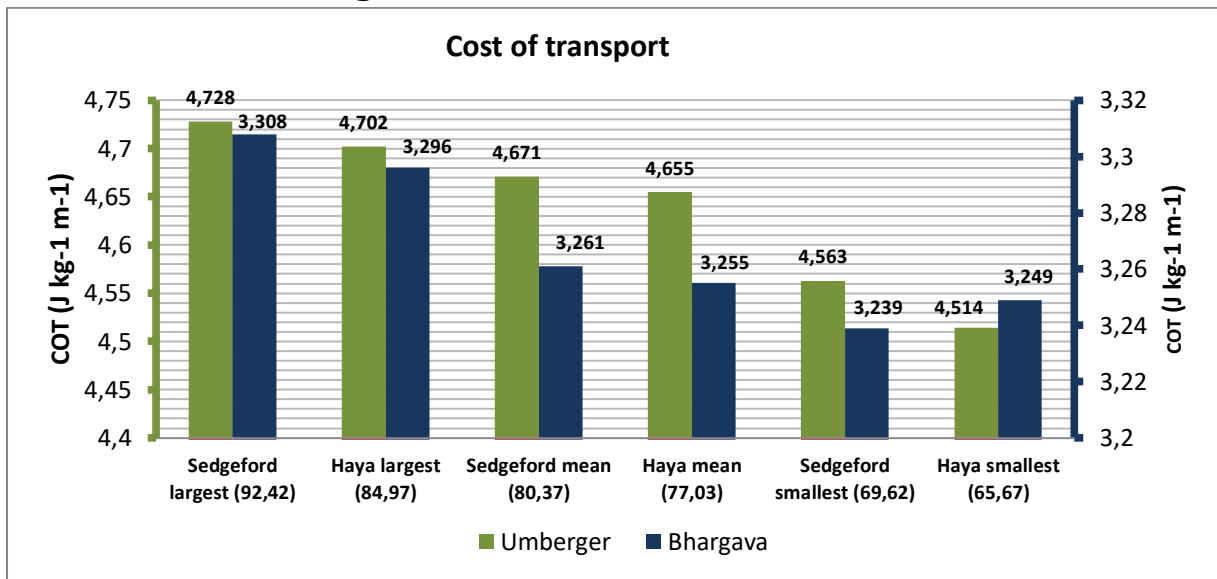


Figure 11: for the two models by Bhargava and Umberger, the cost of transport at 4 m/s is plotted. Notice the color coding of the two models and their respective axis. On the x-axis the models are ordered in decreasing MAXL from left to right, with their respective MAXL in brackets.

Figure 11 shows the cost of transport as a function of MAXL at 4 m/s. Both energy models show the same trend, where a decrease in cost of transport is seen from the largest models to the smallest models. A strong correlation is observed between cost of transport and MAXL ($r=0.97$) for the Umberger model, this correlation is lower for the Bhargava model ($r=0.92$). Reducing the MAXL from the Sedgeford largest (92.42 mm) to the MAXL from the Haya smallest (65.57 mm) reduces the cost of transport with 4.5% if the Umberger model is used. For the Bhargava model this is 1.8% if the Sedgeford largest is compared with the Haya smallest model and 2.1% if the Sedgeford largest is compared with the Sedgeford smallest. The Sedgeford largest model shows the highest absolute cost of transport value and does so for both energy models. The Haya smallest model shows the lowest absolute cost of transport value, but only for the Umberger model. The Bhargava energy model returns a cost of transport value for the Haya smallest model (3.249) that is higher than the Sedgeford smallest model (3.239), while the MAXL of the Haya smallest model is smaller (65.67) than the MAXL of the Sedgeford smallest model (69.62). This forms the only exception to the general trend and, as will be elaborated in the discussion, is treated as outlier. The energy model from Umberger shows absolute higher cost of transport values than the energy model from Bhargava. The Umberger values lie between 4.728 and 4.514, the values of the Bhargava model lie between 3.308 and 3.239. The range in the cost of transport values is largest in the Umberger model (0.214) as opposed to Bhargava (0.069). Since scaling affected the muscle tendon properties of certain muscles acting on the ankle joint, the correlation between cost of transport and MAXL observed for the total body is thought to be related to a change in muscle energy expenditure for those muscles. Table 6 shows the energy expenditure over one stride for all the relevant muscles and for all models, also shown is the correlation coefficient between muscle energy expenditure and MAXL. The correlation between muscle specific energy expenditure and MAXL is negative for the soleus, tibialis posterior and the flexor digitorum muscles. For these muscles, the energy consumption increases with decreasing MAXL. For the other muscles this relationship is positive, cost of transport decreases with decreasing MAXL. For example, for the soleus muscle the maximal difference is observed between the Haya smallest (HS) and Haya largest (HL) models, this maximal difference (1.67) corresponds to a

relative increase in energy consumption (11%) with decreasing MAXL. If the relationship between muscle energy consumption and MAXL is linear, the maximal difference in energy consumption corresponds to a maximal difference in MAXL. This linearity is most evident and for the peroneus brevis, peroneus longus and peroneus tertius, for these muscles the relationship between MAXL and energy consumption is positive and the energy differences are the largest. For the Peroneus brevis muscle energy consumption is at least 70% lower for the smallest MAXL (65.67 mm) when compared with the largest MAXL (92.42 mm). Table 6 also reports the energy stored in the tendon over one stride. In general the energy stored in a specific tendon decreases with decreasing MAXL. This is most significant for the peroneus brevis muscle, where 53.5% less energy is stored in the tendon for the Haya smallest relative to the Sedgford largest. No significant energy storage is observed for the triceps surae muscle group.

Muscles (left leg)	Energy consumed (J)						r	Energy difference (%)
	SL (92.42)	HL (84.97)	SM (80.37)	HM (77.03)	SS (69.62)	HS (65.67)		
Soleus	15.19	15.18	15.25	15.22	16.61	16.85	-0.86	+11%
Gastrocnemius lateralis	6.21	6.31	6.25	6.25	5.41	5.70	0.77	-14.4%
Gastrocnemius medialis	10.38	10.45	10.9	10.94	8.97	8.85	0.70	-19.2%
Tibialis posterior	5.57	6.87	7.25	7.31	6.93	6.81	-0.57	NA
Flexor digitorum	1.83	1.94	2.07	2.14	2.17	2.10	-0.87	+15.5%
Flexor hallucis	2.75	2.76	2.74	2.74	2.66	2.66	0.84	-3.6%
Tibialis anterior	7.30	7.30	7.15	7.20	6.98	6.93	0.94	-5.2%
Peroneus brevis	3.62	2.99	1.56	1.55	1.26	1.07	0.92	-70.5%
Peroneus longus	3.57	3.13	2.96	2.72	1.95	1.79	0.99	-49.8%
Peroneus tertius	2.94	2.71	2.64	2.55	2.23	2.11	0.99	-28%
Extensor digitorum	6.7	6.72	6.54	6.51	6.1	5.74	0.92	-14.6%
Extensor hallucis	2.81	2.72	3.06	3.05	3.13	2.26	0.24	NA
Tendons (left leg)	Energy Stored (J)						r	Energy difference (%)
	SL (92.42)	HL (84.97)	SM (80.37)	HM (77.03)	SS (69.62)	HS (65.67)		
Soleus	4.23	4.22	4.20	4.19	4.19	4.16	0.95	-1.7%
Gastrocnemius lateralis	1.24	1.24	1.23	1.23	1.28	1.27	-0.695	+4.1%
Gastrocnemius medialis	2.89	2.89	2.82	2.81	2.87	2.89	0.12	NA
Tibialis posterior	3.08	2.87	2.72	2.70	2.63	2.64	0.925	-17.1%
Flexor digitorum	0.530	0.538	0.539	0.545	0.560	0.560	-0.972	+5.7%
Flexor hallucis	0.623	0.611	0.594	0.586	0.564	0.559	0.994	-10.3%
Tibialis anterior	0.903	0.902	0.848	0.846	0.833	0.836	0.888	-8.4%
Peroneus brevis	0.399	0.340	0.279	0.276	0.266	0.260	0.906	-53.5%
Peroneus longus	1.353	1.294	1.272	1.244	1.178	1.163	0.996	-16.3%
Peroneus tertius	0.116	0.109	0.106	0.105	0.097	0.092	0.993	-26.1%
Extensor digitorum	1.13	1.08	1.09	1.08	1.02	1.04	0.938	-10.8%
Extensor hallucis	0.284	0.270	0.269	0.266	0.249	0.242	0.980	-17.4%

Table 6: muscle specific energy consumption and tendon energy storage over 1 stride are reported for the left leg and for all models. The models are indicated by their abbreviation (see also table 5) and their MAXL value. The Pearson's correlation coefficient shows the correlation between muscle energy consumption or tendon energy storage and MAXL. In the last column the maximal difference observed between models is reported as percentage. This maximal difference in energy is not always caused by a maximal difference in MAXL. A positive percentage (+) indicates that muscle energy consumption increases with decreasing MAXL; a negative percentage indicates that muscle energy consumption decreases with MAXL. For tendon energy storage this is identical. Where the correlation coefficient is lower than 0.6 the results are deemed to be insignificant (NA).

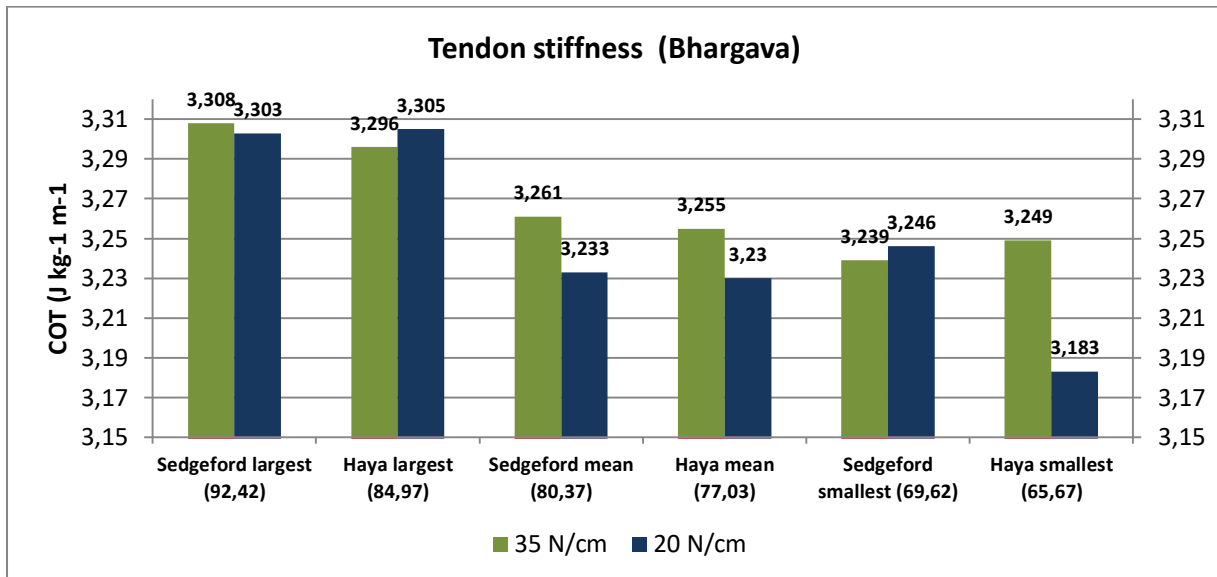
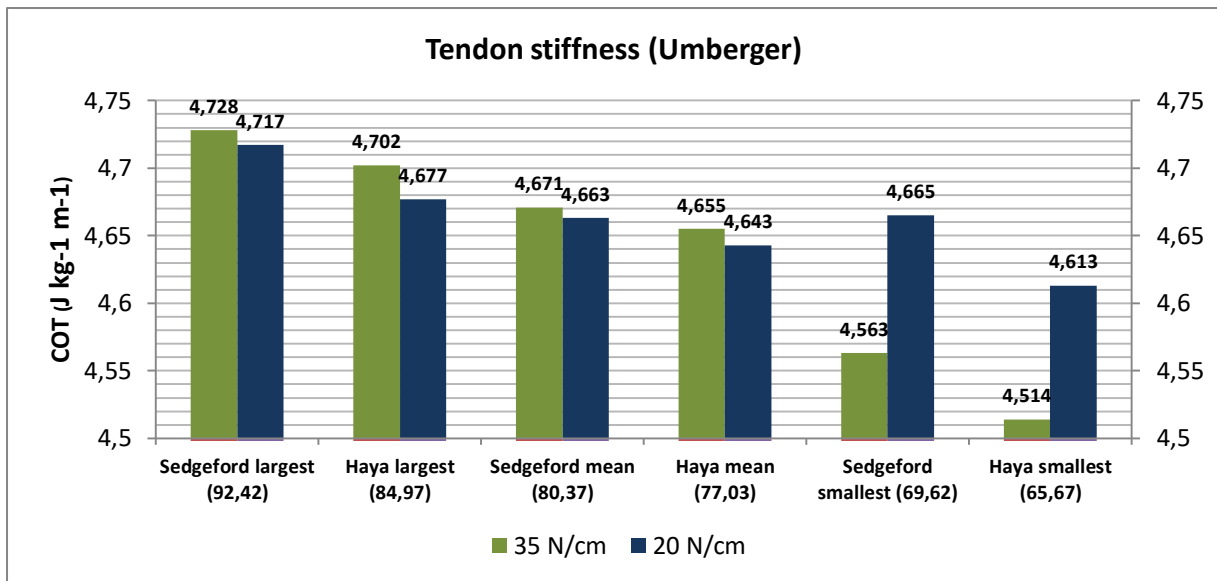


Figure 12: the effect of tendon stiffness on cost of transport at 4 m/s is plotted. For the Umberger energy model, a stiffer tendon (35 N/cm) results in higher cost of transport values for most models except the smallest. For the Sedgeford and Haya smallest models increasing the compliance results in higher cost of transport values. For the Bhargava model the same trend is observed a reduction in stiffness results in lower cost of transport values. The Haya largest and the Sedgeford smallest are the outliers to the same general relationship.

Tendon stiffness of the gastrocnemius medialis, gastrocnemius lateralis and soleus muscles was changed. Figure 12 shows the cost of transport values for the six models with tendon stiffness at 35 N/cm and with tendon stiffness at 20 N/cm. In general, a more compliant tendon (20 N/cm) is correlated to lower cost of transport values ($r=0.80$) for all models using the Umberger model. For the Bhargava model, the same relationship holds ($r=0.83$), but the relationship is not as linear. For the Umberger energy model, the only exception is seen for the Haya and Sedgeford smallest models, where a more compliant tendon results in a larger cost of transport value. When the tendon stiffness is decreased from 35 N/cm to 20 N/cm it results in a maximal 0.53% decrease in cost of transport for most models, but up to 2.24% increase cost of transport for the two smallest models, while using the Umberger model. For the Bhargava model a more compliant tendon results in a maximal 2.03% decrease in cost of transport for the Haya smallest model and a maximal 0.27% increase in cost of transport for the Haya largest model.

4.2 Walking

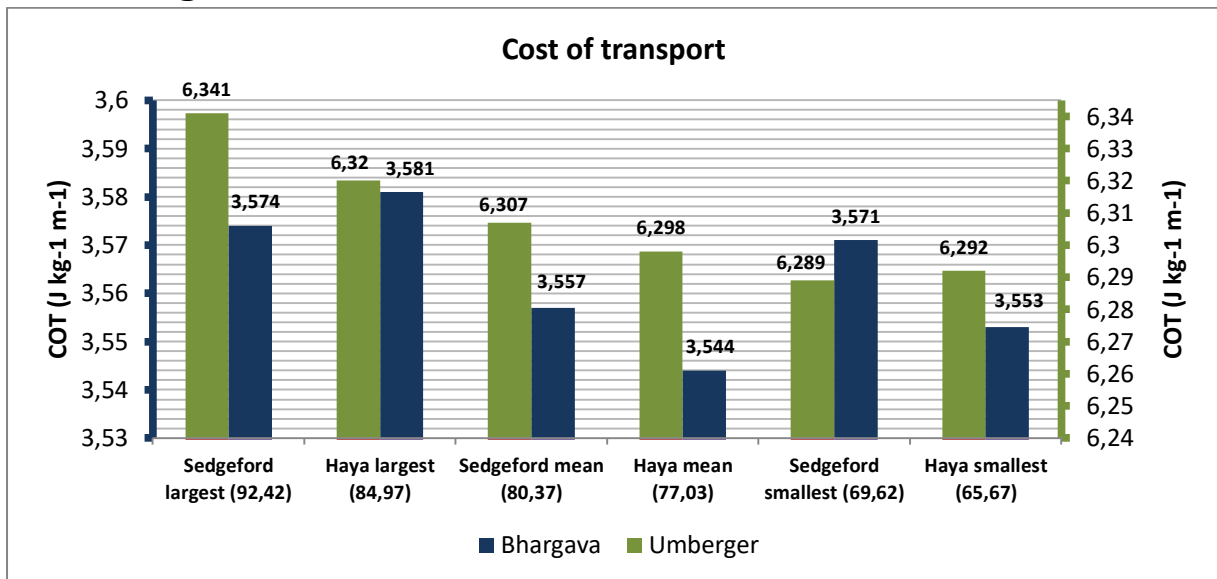


Figure 13: for the two models by Bhargava and Umberger, the cost of transport at 1.33 m/s is plotted. Notice the color coding of the two models and their respective axis. On the x-axis the models are ordered in decreasing MAXL from left to right, with their respective MAXL in brackets.

Figure 13 shows the cost of transport as a function of MAXL at 1.33 m/s. The Umberger model more or less reproduces the same results as observed in figure 11, where a decrease in cost of transport correlates with a decrease in MAXL ($r=0.95$). No significant correlation exists between cost of transport and MAXL when using the Bhargava model ($r=0.49$). The maximal difference in MAXL from the Sedgeford largest to the Haya smallest now produces a reduction of 0.78% in cost of transport using the Umberger model. The energy model from Umberger shows absolute higher cost of transport values than the energy model from Bhargava and also higher cost of transport values than the values observed for the simulation at 4 m/s. According to the results walking at 1.33 m/s is more energy demanding than running at 4 m/s while using the Umberger energy model. The Umberger values lie between 6.341 and 6.289; the range in the cost of transport values in the Umberger model is 0.052. For the Bhargava model the values lie between 3.581 and 3.544 with a range of 0.037. For both these energy models, the reduction in cost is significantly lower than for running. Table 7 shows the energy expenditure over one stride for all the relevant muscles and for all models, also shown is the correlation coefficient between muscle energy expenditure and MAXL. The overall correlation between muscle energy consumption and MAXL is low for most muscles when compared with running. The correlation is positive for all muscles except the tibialis posterior, tibialis anterior, peroneus brevis and the peroneus longus. Positive correlation is significant for the soleus and peroneus tertius muscles. For the soleus muscle a smaller MAXL results in a 4.5% decrease in energy consumption, for the peroneus tertius this is 15%. Negative correlation is not significant enough for any muscle to base conclusions upon. Table 7 also reports the energy stored in the tendon over one stride. In general the same relationship here holds as for running, where a smaller MAXL correlates with less energy stored in the tendon over one stride. This relationship is indicated in the table by a positive correlation coefficient. Largest differences are observed for the flexor digitorum and flexor hallucis, where up to 12.8% less energy is stored as MAXL decreases. As for the energy consumption per muscle, the correlation was very low in general.

Muscles (left leg)	Energy consumed (J)						r	Energy difference (%)
	SL (92.42)	HL (84.97)	SM (80.37)	HM (77.03)	SS (69.62)	HS (65.67)		
Soleus	11.5	11.42	11.32	11.15	11.14	11.01	0.97	-4.5%
Gastrocnemius lateralis	4.984	4.697	4.965	4.882	4.934	4.661	0.39	NA
Gastrocnemius medialis	7.207	7.359	7.283	7.238	7.087	7.126	0.65	-3.8%
Tibialis posterior	6.064	5.993	6.16	6.088	6.245	6.12	-0.61	+4.0%
Flexor digitorum	1.447	1.4	1.427	1.391	1.466	1.347	0.39	NA
Flexor hallucis	1.634	1.598	1.618	1.57	1.625	1.584	0.43	NA
Tibialis anterior	8.384	8.328	8.29	8.244	8.431	8.526	-0.51	NA
Peroneus brevis	2.41	2.234	2.202	2.255	2.453	2.548	-0.51	NA
Peroneus longus	3.124	2.945	2.96	2.821	3.049	3.247	-0.27	NA
Peroneus tertius	1.425	1.313	1.3	1.263	1.239	1.245	0.92	-15%
Extensor digitorum	5.234	5.694	5.547	5.412	5.35	5.26	0.24	NA
Extensor hallucis	1.736	1.673	1.864	1.777	1.633	1.334	0.64	-39.7%
Tendons (left leg)	Energy Stored (J)						r	Energy difference (%)
	SL (92.42)	HL (84.97)	SM (80.37)	HM (77.03)	SS (69.62)	HS (65.67)		
Soleus	7.406	7.416	7.369	7.31	7.339	7.24	0.87	-2.4%
Gastrocnemius lateralis	2.224	2.225	2.25	2.228	2.243	2.222	-0.15	NA
Gastrocnemius medialis	5.028	5.013	5.053	5.03	5.033	4.983	0.41	NA
Tibialis posterior	4.116	4.102	4.105	4.081	4.094	4.082	0.82	-0.9%
Flexor digitorum	1.001	0.973	0.959	0.941	0.921	0.896	0.995	-11.7%
Flexor hallucis	0.998	0.967	0.950	0.93	0.908	0.885	0.997	-12.8%
Tibialis anterior	1.929	1.884	1.862	1.87	1.943	2.017	-0.55	NA
Peroneus brevis	0.586	0.567	0.557	0.553	0.558	0.5666	0.59	NA
Peroneus longus	2.515	2.457	2.428	2.388	2.377	2.373	0.95	-6%
Peroneus tertius	0.176	0.168	0.165	0.163	0.166	0.169	0.49	NA
Extensor digitorum	2.056	2.033	2.01	1.977	2.038	1.963	0.66	-2.4%
Extensor hallucis	0.451	0.436	0.436	0.425	0.4204	0.409	0.98	-7.3%

Table 7: muscle specific energy consumption and tendon energy storage over 1 stride are reported for the left leg and for all models. The models are indicated by their abbreviation (see also table 5) and their MAXL value. The Pearson's correlation coefficient shows the correlation between muscle energy consumption or tendon energy storage and MAXL. In the last column the maximal difference observed between models is reported as percentage. This maximal difference in energy is not always caused by a maximal difference in MAXL. A positive percentage (+) indicates that muscle energy consumption increases with decreasing MAXL; a negative percentage indicates that muscle energy consumption decreases with MAXL. For tendon energy storage this is identical. Where the correlation coefficient is lower than 0.6 the results are deemed to be insignificant (NA).

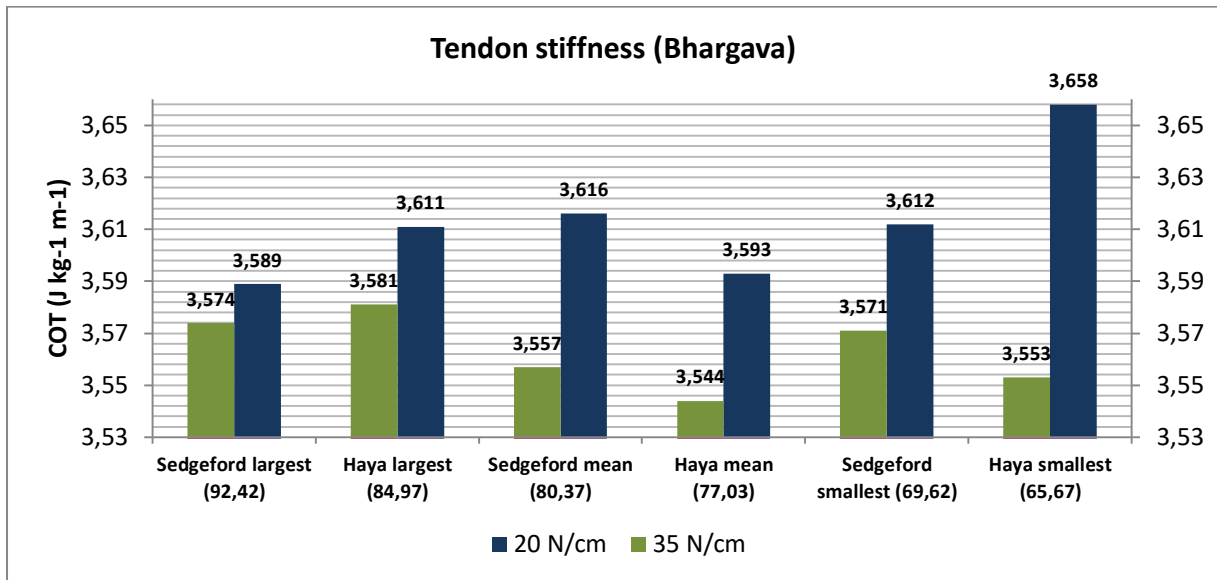
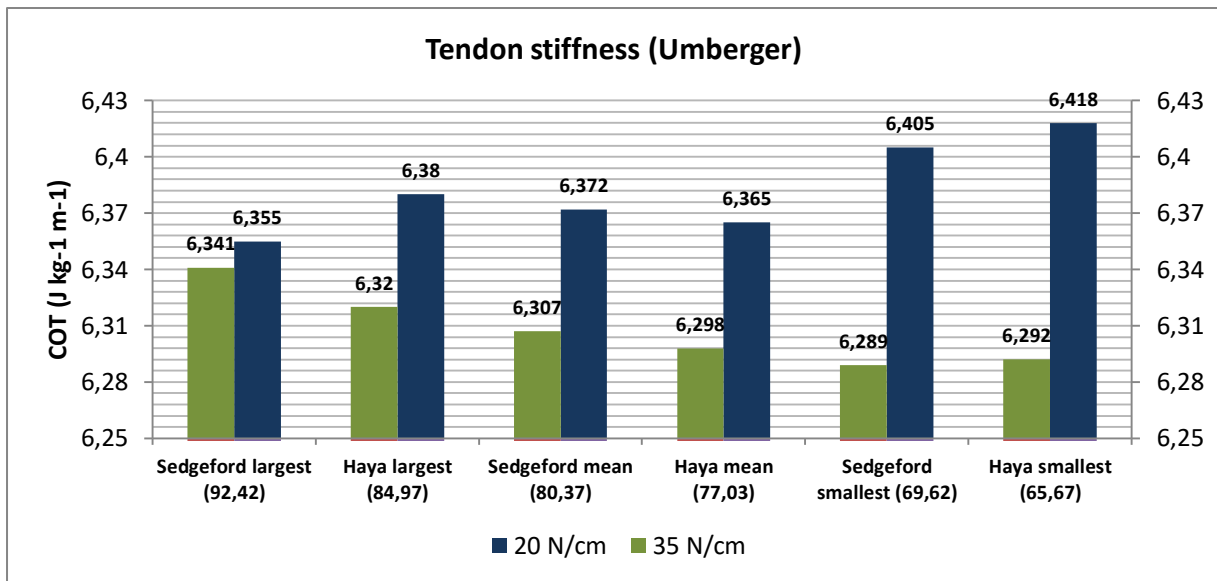


Figure 14: the effect of tendon stiffness on cost of transport at 1.33 m/s is plotted. For the Umberger energy model, a stiffer tendon (35 N/cm) results in lower cost of transport values with decreasing MAXL, reducing the tendon stiffness to 20 N/cm results in higher cost of transport values for all models. For the Bhargava model the same trend is observed a reduction in stiffness results in higher cost of transport values with decreasing MAXL. The Haya largest and the Sedgeford smallest are the outliers to the same general relationship.

Figure 14 shows the cost of transport for the six models at 1.33 m/s while tendon stiffness is varied between 35 and 20 N/cm. For all models a decrease in tendon stiffness results in higher cost of transport values. A more compliant tendon results in the following relationship between cost of transport and MAXL: the cost of transport increases with decreasing MAXL, it is less efficient to have a small calcaneal tuber length when walking at 1.33 m/s and tendon stiffness is low. The maximum range in MAXL between the Sedgeford largest and the Haya smallest is 26.75 mm, this results in a 1% increase in cost of transport for the Haya smallest model relative to the Sedgeford largest model when using the Umberger model. For the Bhargava model a more compliant tendon (20 N/cm) results in a maximal increase in cost of transport of 1.92% between the Sedgeford largest and Haya smallest models. A more compliant tendon inverts the relationship observed at for the stiffer tendon. For a stiffer tendon cost of transport decreased with decreasing MAXL, and for a more compliant tendon cost of transport increases with decreasing MAXL.

5. Discussion

This paper aimed to answer the following research question: does intraspecific variation in calcaneal tuber length affect the metabolic energy expenditure (J/kg/m) of endurance running at 4 m/s? The hypothesis stated that a smaller calcaneal tuber length reduces the Achilles tendon moment arm, thereby increasing the amount of energy stored in the tendon and decrease the cost of transport (J/kg/m). For the simulation performed at 4 m/s, decreasing the MAXL with 2.675 cm reduces the cost of transport with a maximum of 4.5%. For the simulation performed at 1.33 m/s, decreasing the MAXL with 2.675 cm reduces the cost of transport with a maximum of 0.78%. The discussion is structured as follows: section 5.1 discusses the general functioning of the simulations and validates certain settings chosen during the simulations, section 5.2 discusses the results in detail and the main assumption that underlies the hypothesis, and section 5.3 discusses the results in terms of human evolution by comparing the results with used and new literature.

5.1 Optimization performance

In general, the results of the simulations can be evaluated by looking at the cost function value. The cost function value is an indicator of how well the objective function (J) is minimized in terms of its performance criterion, with lower values indicating relative better performance. The framework created by Falisse et al. [71] allows the use of multiple settings. The cost function value allows the user to evaluate which settings create the most ‘realistic’ simulation in terms of optimization. Two important settings are used in this study, namely the initial guess mode and the energy model. Table 8 shows the cost function values for the simulations performed with these varying settings. For the simulations performed at 4 m/s the running initial guess mode, in combination with the Bhargava energy model produces the lowest cost function values. For the simulations performed at 1.33 m/s the walking initial guess mode in combination with the Bhargava energy model produces the lowest cost function values.

Bhargava	Simulations at 4 m/s		Simulations at 1.33 m/s	
	IG walking	IG running	IG walking	IG running
Haya largest	1101	1016	246.9	240.9
Haya mean	1101	1020	240.1	235
Haya smallest	1066	985	243.7	287.7
Sedgeford largest	1102	1039	242.1	290.7
Sedgeford mean	1053	1006	241.7	287.5
Sedgeford smallest	1074	1003	244.3	284.4
Umberger	Simulations at 4 m/s		Simulations at 1.33 m/s	
	IG walking	IG running	IG walking	IG running
Haya largest	1339	1341	439,9	1301
Haya mean	1367	1342	434,8	448.9
Haya smallest	1377	1286	442,9	1196
Sedgeford largest	1376	1363	437,3	1399
Sedgeford mean	1343	1351	434,6	1364
Sedgeford smallest	1374	1307	435,6	454

Table 8: the cost function values are reported for different settings used in the model. Lower cost function values indicate more realistic simulations in terms of the optimization process. For simulations performed at 4 m/s the initial guess (IG) for running in combination with the Bhargava energy model provides the best results. For the simulations performed at 1.33 m/s the initial guess for walking in combination with the Bhargava energy model provides the best results.

The simulations based on the Bhargava energy model resulted in lower cost function values for all simulations, thereby indicating that the results using the Bhargava model would be favorable in terms optimization. Metabolic energy expenditure can be measured experimentally by using for example; calorimetry, pulmonary gas exchange, or heat production during activity. Models rely on the mathematical formulation of thermal heat liberation and mechanical work to estimate energy expenditure. Correlation between models and experimental data is not always high; this is mostly because energy models tend to be based on empirical equations, lacking a direct physiological connection to muscle dynamics. To validate which energy model best approaches reality, comparison studies relate model results with experimental data. One such study [75] compares 7 energy models with experimental data, including the model by Umberger and Bhargava. They found that all 7 models correlated with experimental data with a coefficient of at least 0.9 with the Bhargava model showing the highest correlation coefficient of 0.95. Based on comparison studies and the results in this paper, the Bhargava energy model produces the most realistic results.

Another general point of discussion related to the optimization performance is related to outliers. One such outlier is observed in figure 11, where the Haya smallest model produces a higher cost of transport than the Sedgeford smallest using the Bhargava energy model. Overall the data in this figure implies that cost of transport reduces as a function of reducing MAXL. Since the Haya smallest model has a smaller total calcaneal length (MAXL) than the Sedgeford smallest it would be expected that the corresponding cost of transport is also lower. Must this result then be treated as outlier, or is this result a consequence of the optimization process? In this paper, these outliers are assumed to be the result of the optimization process, during the optimization an optimum for the objective function (J) subject to performance criterion is found. This optimum does not necessarily have to be the most significant optimum ('best fit' to reality); it can also represent a local optimum (see figure 15). It is assumed that most outliers observed in the results represent such a local optimum, which does not represent its true optimum. If this assumption is true, the true optimum would fall then within the expected range of outcomes. This however is never known for sure; the outliers may also just represent a different outcome. Due to the high dimensionality and large amount of states of the optimization this assumption could be not tested.

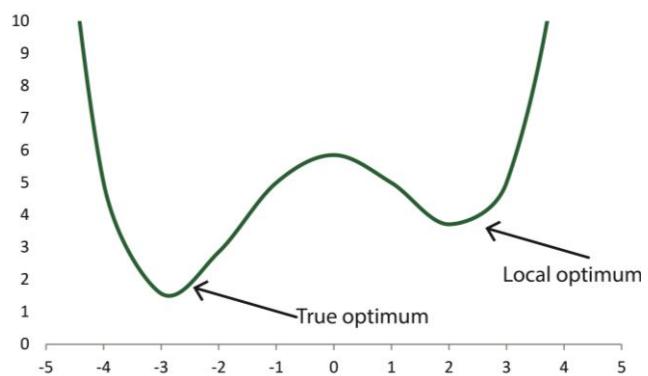


Figure 15: random polynomial function showing the problems that can be encountered while using optimization, where a local optimum may be found instead of the 'true optimum'.

The last point related to the general functioning of the simulations is the contact model, the Hunt Crossley contact model used in the simulations does not change during the scaling. The Hunt Crossley contact model is used to determine the interaction between the feet and the ground, taking into account frictional forces. The model does so by placing spheres at specific locations on the feet, these spheres do not relocate based on the scaling. This is thought to affect the results insignificantly and therefore accepted as such (personal communication with M.Afschrift).

5.2 Results

The Duckworth Laboratory in Cambridge did not have an online catalogue of the material in their collection. This hampered the data collection procedure in such a way that complete control on the sample space could not be guaranteed. The amount of samples taken was enough to get statistically significant differences in calcaneal tuber length; however, no sex or age information was available. Like most other human bones, the morphology of the calcaneus is different between males and females [62, 76], with adult males showing larger calcaneal bones in general than adult females. The two sample groups (Haya and Sedgeford) studied in order to evaluate interregional differences in running economy may be biased towards a certain sex or age. Answering the question as to why athletes from East-Africa (Haya) are so dominant on long distance running competitions loses its statistical validity in the context of provenance. However, the results can still be interpreted in terms of intraspecific variability as the sample space can be treated as random representative of a population. The maximal variation in cost of transport is observed between the models with the maximal variation in MAXL. The maximal variation in MAXL is between the Sedgeford largest and Haya smallest models, with a difference of 2.675 cm. For the simulation performed at 4 m/s, decreasing the MAXL with 2.675 cm reduces the cost of transport with 4.5% if the Umberger energy model is used and 1.8% if the Bhargava energy model is used. Both energy models show a rather linear decrease in cost of transport with decreasing MAXL. The only exception is for the Bhargava model, where the Haya smallest model produced a higher cost of transport value than the Sedgeford smallest model, this was attributed to the optimization performance. For the simulation performed at 1.33 m/s, decreasing the MAXL with 2.675 cm reduces the cost of transport with 0.78% using the Umberger energy model. The simulation at 1.33 m/s using the Bhargava energy model resulted in low correlation between MAXL and cost of transport ($r=0.49$) and is not discussed further. The results show that intraspecific variability in MAXL affects metabolic energy expenditure and that this variability has a more significant effect on endurance running at 4 m/s than walking at 1.33 m/s. Since the relationship between cost of transport and MAXL is insignificant it will not be discussed in detail.

The hypothesis in this paper is based on the assumption that cost of transport reduces due to energy reutilization, as shown in equation 4 and formulated by Scholz [15]. The assumption states that the amount stretching of a tendon and thereby the amount of energy that can be stored and reutilized mainly depends on the Achilles MTU moment arm. Can the relationship between MAXL and cost of transport be attributed to the assumption of tendon energy reutilization? The validity of this assumption can be tested by evaluating the scaling procedure, the muscle energy consumption and tendon energy storage of certain lower leg muscles acting on the ankle. Step one in validating the assumption is to see how the scaling affected muscle tendon parameters and muscle moment arm lengths. If the scaling does not affect tendon moment arm length of the triceps surae the assumption cannot be validated, since the tendon moment arm length determines the muscle tendon dynamics that are linked to the assumption. The most important factor that influenced the scaling step is the calcaneum mesh. The calcaneum mesh (see figure 9) includes the 5 metatarsals and 5 tarsi (cuboid, navicular and 3 cuneiforms). The scaling of the entire mesh was expected to affect moment arm length and muscle tendon properties of the triceps surae since these muscles attach to that mesh. First the muscle tendon parameters were compared. The muscle tendon parameters provide initial insight in how muscle dynamics differ between the six models. The results showed that muscle tendon parameters changed for certain lower leg muscles, but not for the triceps surae, as was

expected. Tendon slack length, optimal fiber length, maximal contraction velocity, maximal isometric force and optimal pennation angles are all identical for the triceps surae muscles in all six models. Second, the moment arm lengths of the six models were compared. No differences were found, the moment arm lengths of the gastrocnemius medialis, gastrocnemius lateralis and soleus are 4.35, 4.32 and 2.81 cm respectively for all six models. Scaling the calcaneum in OpenSim did not affect the moment arm length of these three plantarflexing muscles. Third, muscle specific energy consumption per gait cycle was evaluated. The results showed that for the simulations performed at 4 m/s the reduction in cost of transport is likely the result of a decrease of energy consumption in the peroneus brevis, peroneus longus and peroneus tertius (table 6), which are relative weak plantarflexing muscles. No large differences in muscle energy consumption are observed between the six models for the triceps surae. The reduction in energy consumption in the peroneus brevis and peroneus longus is related to the scaling of the calcaneum, the peroneus muscles all attach to the anterior side of the calcaneum mesh (figure 9) and scaling of the calcaneum thus affected these muscles. In reality the peroneus muscles attach to the metatarsals and varying calcaneum size would not affect the properties of those muscles. What the exact relationship is between the reduction in cost of transport, a smaller calcaneum and the peroneus muscles remains unclear. Most other muscles acting on the ankle joint also showed a reduction in energy consumption with a decrease in MAXL, only the soleus and the flexor digitorum showed an increase in energy consumption with a decrease in MAXL. Fourth, energy storage in the tendons was evaluated. Energy storage in the tendons over one stride also provided no further evidence for a relationship between the triceps surae and cost of transport. Over one stride energy storage in the tendon increased for the gastrocnemius lateralis and flexor digitorum, for the other tendons energy storage decreased with decreasing MAXL. This is not in line with the stated hypothesis that energy storage in a tendon increases with decreasing MAXL.

What has now become evident is that the hypothesis is correct, but the main assumption supporting this hypothesis was not proven. The reduction in cost of transport with smaller calcaneal tuber length is observed, but this is mainly caused by changes in muscle dynamics of the peroneus brevis peroneus tertius and peroneus longus. As this was attributed to the scaling of the calcaneum a different approach was used. In this sensitivity experiment the tendon attachment of the gastrocnemius medialis, gastrocnemius lateralis and soleus muscles was manually shifted 2.7 cm posterior in the x-direction from its attachment point in the calcaneum, this corresponds to the maximal increase in calcaneal tuber length observed in the data. The calcaneum is not scaled in this experiment, in this way the muscle tendon dynamics of the triceps surae muscle group change without affecting muscle tendon dynamics of other muscles acting on the ankle joint.

Muscle	Moment arm (cm)	
	'Normal'	'Tendon shifted posterior'
Medial gastrocnemius	4.35	4.37
Lateral gastrocnemius	4.32	4.34
Soleus	2.81	2.86

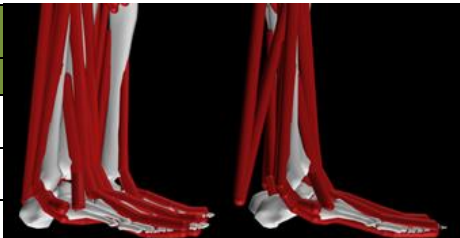


Table 9: the moment arm lengths for the triceps surae muscles in cm are shown. Evident is that when the tendon is shifted posterior by 2.7 cm moment arm length increases slightly. On the right is the shifting visualized, with the right model showing increased distance between the ankle joint and the triceps surae attachment point to the calcaneum.

Muscle tendon parameters did not differ between these two models. However, when the tendon attachment locations of the triceps surae muscle group to the calcaneum are manually displaced with 2.7 cm posteriorly, the static moment arm lengths do vary between the two models above (see table 9). For the model where the tendon is shifted posterior the moment arm increases slightly. Cost of transport is higher when the moment arm is longer; 4.668 for the 'tendon shifted posterior' model as opposed to 4.596 for the 'normal' model, which is a reduction of 1.57%. For the Bhargava energy model this reduction is 1.84%. Smaller moment arm lengths of the triceps surae lead to a reduction in cost of transport, this reduction is thought mainly to arise from reduced muscle energy consumption of the gastrocnemius lateralis (-8.6%), tibialis anterior (-27.4%), peroneus brevis (-46.3%), peroneus longus (-5.4%), peroneus tertius (-8.88%) and extensor digitorum (-25.46%) for the 'normal' model when compared with the 'tendon shifted posterior' model. Muscle energy consumption increased for the gastrocnemius medialis (+1.65%), soleus (+160.8%), tibialis posterior (2.8%), flexor digitorum (+15.24%) and extensor hallucis (+11.1%) muscles for the 'normal' model when compared with the 'tendon shifted posterior' model. For a smaller moment arm total energy storage in the triceps surae tendons increases over one stride (figure 16), as is for the flexor digitorum and flexor hallucis muscles. Tendon energy storage increases with 0.49% for the gastrocnemius medialis, with 4.35% for the gastrocnemius lateralis and with 24% for the soleus muscle. Increased energy storage in the soleus muscle does not correlate with reduced muscle energy consumption however as energy consumption in the soleus muscle is 160% higher and tendon energy storage is 24% higher for the smaller moment arm. The link between tendon energy storage and muscle energy reduction remains unproven. Perhaps the elastic energy stored in the triceps surae muscles is not directly returned to those muscles but indirectly to for example the tibialis anterior and peroneus brevis muscles which show the largest decrease in muscle energy consumption.

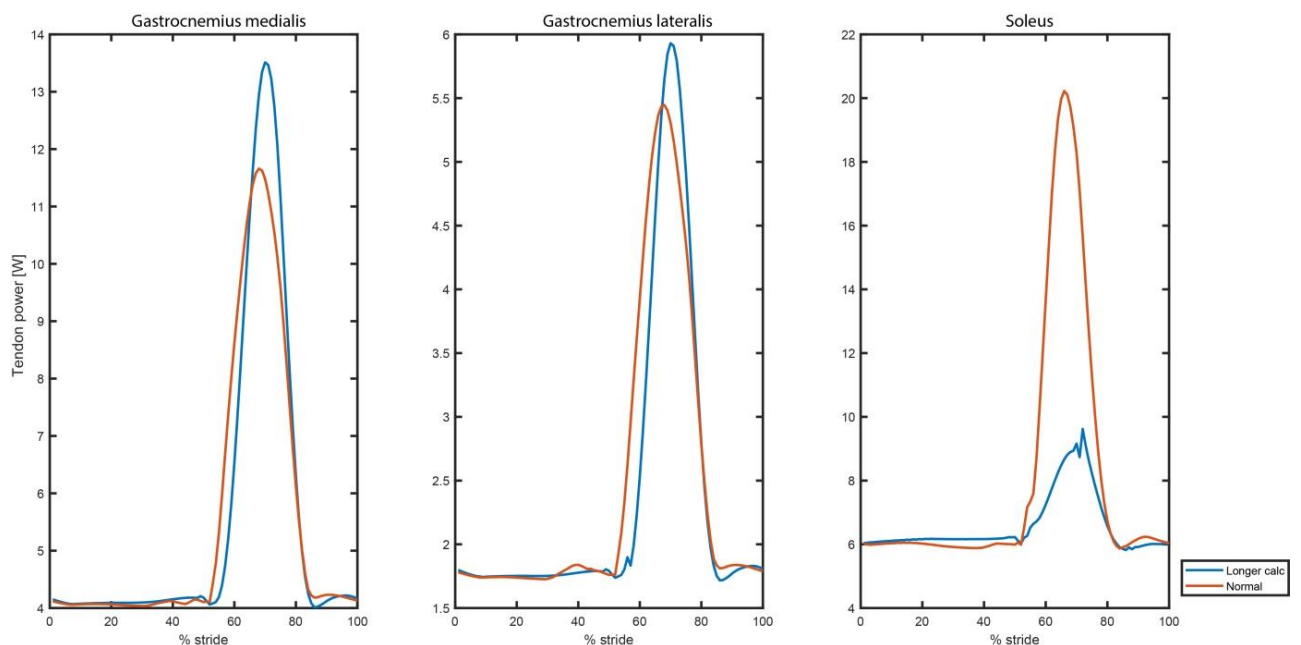


Figure 16: tendon energy storage for the triceps surae of the left leg. Energy storage is similar for the gastrocnemius muscles for both models. For the soleus energy storage is significantly higher for a smaller moment arm.

Not only was the effect of moment arm on cost of transport investigated. According to equation 4 energy storage also increases as a function of tendon compliance (u_{max}) and tendon slack length (l_{se0}). Decoupled from the main hypothesis, a sensitivity experiment was performed to evaluate the effect of tendon stiffness on cost of transport. Tendon stiffness in the model was set to 35 N/cm as a standard value with shift (0). The shift is an added function to describe the tendon force-strain curve. As most phenomenological curves in the Hill muscle model, the tendon force is normalized to tendon slack length. For a different tendon stiffness, the tendon strain relationship changes. The shift function shifts the curve in such a way that normalized tendon force would be the same as with the standard tendon stiffness at a normalized tendon length of 1. The results showed that increased tendon compliance resulted in lower cost of transport for most models at 4 m/s. This is in agreement with literature [77-79], a more compliant tendon is thought to allow a muscle to remain near its optimal muscle fiber length during contraction, and muscle shortening occurs at much slower speed, thus decreasing energy expenditure. Higher tendon stiffness requires the muscle fascicles to operate with higher shortening velocities thereby increasing the heat production and energy consumption. A more compliant tendon, however, may interfere with the direct transmission of muscle shortening to joint movement. Thus, in movements where the pre-stretch is small, such as in walking, a more compliant tendon reduces the force transmission to joint moment, and possibly increasing the metabolic energy expenditure instead of reducing it. The results showed that increased tendon compliance for walking resulted in higher cost of transport. This is attributed to the reduced transmission of shortening muscle force to joint moment. It is thought that as for most muscle tendon properties there must be optimal tendon stiffness as both a too stiff or too compliant tendon results in an increase in cost of transport. Besides moment arm and tendon stiffness tendon slack length might also be a factor determining the energy stored in the tendon. The effect of tendon slack length was not investigated in this research, but according to literature, a longer tendon slack length is associated with better running economy in endurance runners [80].

5.3 Endurance running evolution

From the results it is now evident, albeit not causally supported by the stated assumption, that a smaller calcaneal tuber reduces energy consumption. The question that now remains is whether fossil record agrees with these results. Based on the calcaneal fragments described in literature, do we see a significant change in calcaneal (tuber) length when considering the transition from *Australopithecines* to *Homo erectus* to *Homo sapiens*? First the results can be compared with Scholz [15], which formulated the relationship between Achilles tendon reutilization and running economy for modern humans. Raichlen [14] took it one step further and compared calcaneal data as proxy for tendon moment arm between *Neanderthals* and early *Homo sapiens*.

Scholz measured the moment arm length on several participating athletes and measured running economy (Vo_2) at 16 km/h. Here the moment arm length of the participants varied between 5.3 and 4.2 cm. If only the contribution of energy storage in the Achilles tendon is considered, they estimate that a decrease of 10% in moment arm length would result in a 4.2 ml/kg/min difference. Participant 11 was measured to have a moment arm of 4.9 cm with a corresponding Vo_2 of 50.5 ml/kg/min. Participant 7 was measured to have a moment arm of 4.4 cm, which had a Vo_2 of 45.4 ml/kg/min. A 10% decrease in moment arm results in a 10% decrease in cost, which is largely attributed to energy storage in the tendon and in line with their estimations. The relationship between calcaneal morphology and running economy was also investigated by Raichlen [14]. They investigated the relationship between calcaneal size and running economy for human evolution.

Raichlen proposed to use calcaneal tuber length as skeletal correlate of Achilles tendon moment arm. They measured calcaneal tuber lengths on *Neanderthals* and early *Homo sapiens* and corrected for body mass. They found that *Neanderthals* had the largest relative calcaneal tuber lengths, and thereby less economic running capabilities (Vo_2). Modern humans (N=8) had an average calcaneal tuber length of 13.37 and Vo_2 of 51.17. Fossil early *Homo sapiens* (N=11) had an average calcaneal tuber length of 13.94 and Vo_2 of 52.88. *Neanderthals* (N=7) had an average calcaneal tuber length of 14.52 and Vo_2 of 56.91. Thus a maximal reduction of 1.15 cm in body mass corrected calcaneal tuber length results in a 7.1% decrease in running economy between *Neanderthals* and modern humans. This is under the assumption that the muscle tendon dynamics did not differ between *Neanderthals* and modern humans. It is hypothesized that *Neanderthals* had reduced endurance running capabilities due to its environment. *Neanderthals* lived and hunted in relative colder climates, running prey to exhaustion would not have been applicable under those circumstances. Both studies agree with the results in this paper that a reduction in calcaneal tuber length reduces Achilles tendon moment arm and overall metabolic energy consumption (Vo_2 or cost of transport). However, both studies demonstrate a larger reduction in energy consumption with even smaller differences in moment arm length. This large a difference is not observed in this study, here a maximal difference in CTL of 1.6 cm results in a range of energy decrease between 4.5% and 1.57% depending on the settings and choice of energy model. The relative large difference between the two studies is attributed to the non-sensitivity of the model to scaling. Moment arm did not vary when scaling the calcaneum mesh in the x-direction and minimally when the tendon was shifted posterior manually. When moment arm did change, energy storage markedly increased for the soleus with 24% over one stride, this however did not result in decreased energy consumption of the corresponding muscle. The direct relationship between tendon energy storage and muscle energy consumption remains unproven.

In the background information it was estimated the *Homo erectus* was the first hominin with relatively enhanced endurance running capabilities. Human foot evolution was explained in a three step fashion from early *Ardipithecus* to *Australopithecus* to *Homo*. The first stage describes the locomotive capabilities of *Ardipithecus*, who belongs to the same sub-tribe as *Australopithecus*. *Ardipithecus* shows relatively more adaptations to arboreality than to bipedalism. But general agreement is that *Ardipithecus ramidus* was occasional bipedal[81]. The genus *Australopithecus* is believed to be an intermediate stage when considering the evolution of the foot to bipedal walking and running. It was claimed that *Australopithecus* was insignificantly arboreal around 3 million years ago. The third stage is concerned with early species of the genus *Homo*. Based on fossil trackways and some foot bones, it is thought that *Homo erectus* would have been a rather efficient endurance runner compared with *Australopithecus*. This general three step fashion of feet evolution is directional towards enhanced bipedalism and endurance running. However, when looking at the evolution of solely the calcaneum, the story becomes more complex. From the study from Raichlen et al, it is now know that *Neanderthals* were not efficient endurance runners, which may be attributed to the climate it dominantly lived in and the hunting techniques used. This does not fit with a directional evolution of the human foot towards enhanced endurance running. A review paper by [81] describes the evolution of the human feet. Existing fossil data on the calcaneum is summarized and in decreasing order total calcaneal length is given for *Neanderthals* (0.2 Ma), early *Homo* (0.43 Ma) from Spain, early *Homo* (0.26 Ma) from China, *Paranthropus* (2.36 Ma), *A.afarensis* (3.2 Ma), *Homo naledi* (0.24 Ma), and *A.sediba* (1.98 Ma). There is no correlation whatsoever

between total calcaneal length and time, calcaneal length does not decrease linearly with time. Thomas Prang [82] mainly looked at calcaneal robusticity as indicator for enhanced bipedalism, under the assumption that a robust calcaneum is a more adapted trait to bipedal walking and running. He found that the robusticity of *A. sediba* calcanei was reduced and similar to those of apes, while calcaneal tuber length was relatively human-like. The evolution of the calcaneum does not appear to be as simple as a three step fashion towards enhanced endurance running capabilities. This leads to several speculations. It may indicate that evolution of the calcaneum towards enhanced endurance running is not directional; with several reversals occurring or that these traits evolved separately between different hominin species. Whether a shorter calcaneus is an adaption to endurance running cannot be concluded for sure. Lacking is fossil calcaneal data attributed to early *Homo* species such as *Homo erectus*. Accurate chronologic fossil data on calcanei between 4 and 0.5 Ma is needed in order to evaluate the evolution of the calcaneum.

Conclusion

Intraspecific variability in calcaneal length affects cost of transport (J/kg/m). A reduction of 2.675 cm in total calcaneal length (MAXL) reduces cost of transport overcome with a maximum of 4.5%. The scaling method applied in this paper did not affect moment arm lengths and muscle tendon parameters of the triceps surae. Consequently, the reduction in cost of transport is not attributed to the storage and reutilization of energy in the triceps surae. Energy consumption of lower leg muscles over one stride demonstrates that the reduction in cost of transport is likely the result of reduced muscle energy consumption in the peroneus brevis and peroneus longus muscles. Significant energy storage in the triceps surae was not observed. Scaling of the calcaneum mesh had significant effect on all modeled muscles acting on the ankle joint, with the exception of the triceps surae. By manually shifting the attachment point of the triceps surae to the calcaneum posterior it was tried to negate the effects scaling on other muscles acting on the ankle joint. This resulted in a lengthening of the moment arm of the triceps surae. Cost of transport was maximally 1.84% lower for a shorter moment arm length. Energy storage in the triceps surae tendons increased over one stride in comparison with a larger moment arm. Muscle specific energy consumption for the triceps surae did not decrease over one stride however, and muscle energy consumption for the soleus muscle increased 160%. The relationship between tendon energy storage and muscle energy consumption remains unproven. The sensitivity of the triceps surae to scaling is not high enough, scaling did not affect the moment arm of the triceps surae and did not change the muscle tendon parameters. Literature demonstrates that the evolution of the calcaneum is complex, and that based on the fossil data that is present, no conclusive link between calcaneal size and enhanced endurance running can be proven yet.

Future research should aim to gather more experimental data, including sex and age control. In this way the statistical significance is more robust and perhaps interregional differences can be determined with more certainty. The calcaneum mesh must be separated into the calcaneum, the tarsi and metatarsals. In this way the effect of calcaneal size on muscle tendon parameters of the triceps surae can be examined without changing muscle tendon parameters of the other muscles acting on the ankle. 3D scans of the calcaneum should be considered to improve objectivity of the scaling. Lastly, the focus in the simulation must shift in the exact relationship between tendon energy storage and muscle energy consumption. Interesting is also to look deeper into the differences between intrinsic tendon properties such as tendon slack length and tendon stiffness and compare the effect of those factors with that of moment arm length.

Acknowledgements

I spent two weeks in total at the University of Leuven (KU Leuven), where I worked on the simulation part of this paper. I wish to express my gratitude to Friedl de Groote, who welcomed me to work at their campus and aided me in the continuation of my thesis. I wish to thank A.Falisse and especially M.Afschrift from KU Leuven with their tremendous help on the simulations and scripting in MATLAB. I thank J.vanDieen from the VU Amsterdam for setting up my connections with Leuven, his knowledge on statistics and biomechanics and his review during the process. I thank the Duckworth Laboratory, University of Cambridge, for permission to study material within its collections. I wish to thank the Hans de Bruijn foundation for their grant, allowing me to gather experimental data at the Duckworth Laboratory. I thank Jelle Reumer for his guidance and critical reviews, and the department Earth, Life & Climate for their financial support. Lastly, I thank D.Slump, P.Slump, and H.Beijleveld for their review and support along the process.

Works Cited

1. Bramble, D.M. and D.E. Lieberman, *Endurance running and the evolution of Homo*. Nature, 2004. **432**(7015): p. 345.
2. Lieberman, D.E. and D.M. Bramble, *The evolution of marathon running*. Sports Medicine, 2007. **37**(4-5): p. 288-290.
3. Larsen, H. and A. Sheel, *The Kenyan runners*. Scandinavian journal of medicine & science in sports, 2015. **25**: p. 110-118.
4. Balke, B. and C. Snow, *Anthropological and physiological observations on Tarahumara endurance runners*. American Journal of Physical Anthropology, 1965. **23**(3): p. 293-301.
5. Pilbeam, D., *The descent of hominoids and hominids*. Scientific American, 1984. **250**(3): p. 84-97.
6. Lieberman, D.E., et al., *Brains, brawn, and the evolution of human endurance running capabilities*, in *The first humans—origin and early evolution of the genus homo*. 2009, Springer. p. 77-92.
7. Steudel-Numbers, K.L., T.D. Weaver, and C.M. Wall-Scheffler, *The evolution of human running: effects of changes in lower-limb length on locomotor economy*. Journal of Human Evolution, 2007. **53**(2): p. 191-196.
8. Kram, R. and C.R. Taylor, *Energetics of running: a new perspective*. Nature, 1990. **346**(6281): p. 265-267.
9. Ker, R., et al., *The spring in the arch of the human foot*. Nature, 1987. **325**(6100): p. 147.
10. Holowka, N.B. and D.E. Lieberman, *Rethinking the evolution of the human foot: Insights from experimental research*. Journal of Experimental Biology, 2018. **221**(17): p. jeb174425.
11. Rolian, C., et al., *Walking, running and the evolution of short toes in humans*. Journal of Experimental Biology, 2009. **212**(5): p. 713-721.
12. Latimer, B. and C.O. Lovejoy, *The calcaneus of Australopithecus afarensis and its implications for the evolution of bipedality*. American Journal of Physical Anthropology, 1989. **78**(3): p. 369-386.
13. Jungers, W.L., *Relative joint size and hominoid locomotor adaptations with implications for the evolution of hominid bipedalism*. Journal of Human Evolution, 1988. **17**(1-2): p. 247-265.
14. Raichlen, D.A., H. Armstrong, and D.E. Lieberman, *Calcaneus length determines running economy: implications for endurance running performance in modern humans and Neandertals*. Journal of human evolution, 2011. **60**(3): p. 299-308.
15. Scholz, M.N., et al., *Running biomechanics: shorter heels, better economy*. Journal of Experimental Biology, 2008. **211**(20): p. 3266-3271.

16. Kivell, T.L. and D. Schmitt, *Independent evolution of knuckle-walking in African apes shows that humans did not evolve from a knuckle-walking ancestor*. Proceedings of the National Academy of Sciences, 2009. **106**(34): p. 14241-14246.
17. Richmond, B.G., D.R. Begun, and D.S. Strait, *Origin of human bipedalism: the knuckle-walking hypothesis revisited*. American Journal of Physical Anthropology: The Official Publication of the American Association of Physical Anthropologists, 2001. **116**(S33): p. 70-105.
18. Sockol, M.D., D.A. Raichlen, and H. Pontzer, *Chimpanzee locomotor energetics and the origin of human bipedalism*. Proceedings of the national academy of sciences, 2007. **104**(30): p. 12265-12269.
19. Carrier, D.R., et al., *The energetic paradox of human running and hominid evolution [and comments and reply]*. Current Anthropology, 1984. **25**(4): p. 483-495.
20. Raichlen, D.A., et al., *Laetoli footprints preserve earliest direct evidence of human-like bipedal biomechanics*. PLoS One, 2010. **5**(3): p. e9769.
21. Zollikofer, C.P., et al., *Virtual cranial reconstruction of Sahelanthropus tchadensis*. Nature, 2005. **434**(7034): p. 755.
22. Böhme, M., et al., *A new Miocene ape and locomotion in the ancestor of great apes and humans*. Nature, 2019. **575**(7783): p. 489-493.
23. Faith, J.T. and A.K. Behrensmeyer, *Climate change and faunal turnover: testing the mechanics of the turnover-pulse hypothesis with South African fossil data*. Paleobiology, 2013. **39**(4): p. 609-627.
24. David, R., *Functional Tradeoffs in Specialization for Fighting versus Running*. 2002.
25. Carrier, D.R., *The short legs of great apes: evidence for aggressive behavior in australopiths*. Evolution, 2007. **61**(3): p. 596-605.
26. Carrier, D.R. and C. Cunningham, *The effect of foot posture on capacity to apply free moments to the ground: implications for fighting performance in great apes*. Biology open, 2017. **6**(2): p. 269-277.
27. Liebenberg, L., *The relevance of persistence hunting to human evolution*. Journal of Human Evolution, 2008. **55**(6): p. 1156.
28. Watanabe, H., *Running, creeping and climbing: a new ecological and evolutionary perspective on human locomotion*. The Australian Journal of Anthropology, 1971. **8**(1): p. 1.
29. Liebenberg, L., *Persistence hunting by modern hunter-gatherers*. Current Anthropology, 2006. **47**(6): p. 1017-1026.
30. Wilson, R.S. and R.S. James, *Constraints on muscular performance: trade-offs between power output and fatigue resistance*. Proceedings of the Royal Society of London. Series B: Biological Sciences, 2004. **271**(suppl_4): p. S222-S225.
31. Selinger, J.C., et al., *Humans can continuously optimize energetic cost during walking*. Current Biology, 2015. **25**(18): p. 2452-2456.
32. Pablos, A., *The foot in the Homo fossil record*. Mitteilungen der Gesellschaft für Urgeschichte, 2015. **24**(11).
33. Lovejoy, C.O., et al., *Combining prehension and propulsion: the foot of Ardipithecus ramidus*. science, 2009. **326**(5949): p. 72-72e8.
34. Susman, R.L., J.T. Stern Jr, and W.L. Jungers, *Arboreality and bipedality in the Hadar hominids*. Folia primatologica, 1984. **43**(2-3): p. 113-156.
35. Zipfel, B., et al., *The foot and ankle of Australopithecus sediba*. Science, 2011. **333**(6048): p. 1417-1420.
36. Susman, R.L. and J.T. Stern, *Functional morphology of Homo habilis*. Science, 1982. **217**(4563): p. 931-934.
37. Pontzer, H., et al., *Locomotor anatomy and biomechanics of the Dmanisi hominins*. Journal of human evolution, 2010. **58**(6): p. 492-504.
38. Hatala, K.G., et al., *Footprints reveal direct evidence of group behavior and locomotion in Homo erectus*. Scientific reports, 2016. **6**: p. 28766.

39. Van Dam, J.A., et al., *Long-period astronomical forcing of mammal turnover*. Nature, 2006. **443**(7112): p. 687-691.
40. Hamill, J. and K.M. Knutzen, *Biomechanical basis of human movement*. 2006: Lippincott Williams & Wilkins.
41. Dugan, S.A. and K.P. Bhat, *Biomechanics and analysis of running gait*. Physical Medicine and Rehabilitation Clinics, 2005. **16**(3): p. 603-621.
42. Novacheck, T.F., *The biomechanics of running*. Gait & posture, 1998. **7**(1): p. 77-95.
43. Hill, A.V., *The heat of shortening and the dynamic constants of muscle*. Proceedings of the Royal Society of London. Series B-Biological Sciences, 1938. **126**(843): p. 136-195.
44. Thelen, D.G., F.C. Anderson, and S.L. Delp, *Generating dynamic simulations of movement using computed muscle control*. Journal of biomechanics, 2003. **36**(3): p. 321-328.
45. Raasch, C.C., et al., *Muscle coordination of maximum-speed pedaling*. Journal of biomechanics, 1997. **30**(6): p. 595-602.
46. Thelen, D.G., *Adjustment of muscle mechanics model parameters to simulate dynamic contractions in older adults*. J. Biomech. Eng., 2003. **125**(1): p. 70-77.
47. John, C., *Complete Description of the Thelen2003Muscle Model*. 2011.
48. Anderson, F.C. and M.G. Pandy, *A dynamic optimization solution for vertical jumping in three dimensions*. Computer methods in biomechanics and biomedical engineering, 1999. **2**(3): p. 201-231.
49. Sparrow, W. and K. Newell, *Metabolic energy expenditure and the regulation of movement economy*. Psychonomic Bulletin & Review, 1998. **5**(2): p. 173-196.
50. Bhargava, L.J., M.G. Pandy, and F.C. Anderson, *A phenomenological model for estimating metabolic energy consumption in muscle contraction*. Journal of biomechanics, 2004. **37**(1): p. 81-88.
51. Umberger, B.R., K.G. Gerritsen, and P.E. Martin, *A model of human muscle energy expenditure*. Computer methods in biomechanics and biomedical engineering, 2003. **6**(2): p. 99-111.
52. Umberger, B.R., *Stance and swing phase costs in human walking*. Journal of the Royal Society Interface, 2010. **7**(50): p. 1329-1340.
53. Saibene, F. and A.E. Minetti, *Biomechanical and physiological aspects of legged locomotion in humans*. European journal of applied physiology, 2003. **88**(4-5): p. 297-316.
54. Donelan, J.M., R. Kram, and A.D. Kuo, *Simultaneous positive and negative external mechanical work in human walking*. Journal of biomechanics, 2002. **35**(1): p. 117-124.
55. Kuo, A.D., J.M. Donelan, and A. Ruina, *Energetic consequences of walking like an inverted pendulum: step-to-step transitions*. Exercise and sport sciences reviews, 2005. **33**(2): p. 88-97.
56. Doral, M.N., et al., *Functional anatomy of the Achilles tendon*. Knee Surgery, Sports Traumatology, Arthroscopy, 2010. **18**(5): p. 638-643.
57. Rosso, C. and V. Valderrabano, *Biomechanics of the Achilles Tendon*. 2010.
58. van Ingen Schenau, G., *An alternative view of the concept of utilisation of elastic energy in human movement*. Human Movement Science, 1984. **3**(4): p. 301-336.
59. Hoggett, R., *Sedgeford Historical and Archaeological Research Project, 2000: Fifth Interim Report*. Norfolk Archaeology, 2001. **43**(4): p. 681-682.
60. Haas, J., et al., *Standards for Data Collection from Human Skeletal Remains: Proceedings of a Seminar at the Field Museum of Natural History, Organized by Jonathan Haas*. 1994: Arkansas Archeological Survey.
61. Schwartz, J.H., *Skeleton Keys: An Introduction to Human Skeletal Morphology, Development, and Analysis*. 1995: Oxford University Press.
62. Bidmos, M., *Metrical and non-metrical assessment of population affinity from the calcaneus*. Forensic science international, 2006. **159**(1): p. 6-13.

63. İlhan, O., et al., *Morphometric Measurements of Calcaneus; Boehler's angle and bone length estimation*. Cumhuriyet Üniversitesi Fen-Edebiyat Fakültesi Fen Bilimleri Dergisi, 2017. **38**(2): p. 256-263.
64. Seth, A., et al., *OpenSim: Simulating musculoskeletal dynamics and neuromuscular control to study human and animal movement*. PLoS computational biology, 2018. **14**(7): p. e1006223.
65. Delp, S.L., et al., *OpenSim: open-source software to create and analyze dynamic simulations of movement*. IEEE transactions on biomedical engineering, 2007. **54**(11): p. 1940-1950.
66. Sherman, M.A., A. Seth, and S.L. Delp, *Simbody: multibody dynamics for biomedical research*. Procedia lutam, 2011. **2**: p. 241-261.
67. Seth, A., et al., *OpenSim: a musculoskeletal modeling and simulation framework for in silico investigations and exchange*. Procedia lutam, 2011. **2**: p. 212-232.
68. Rajagopal, A., et al., *Full-body musculoskeletal model for muscle-driven simulation of human gait*. IEEE transactions on biomedical engineering, 2016. **63**(10): p. 2068-2079.
69. Lee, L.-F. and B.R. Umberger, *Generating optimal control simulations of musculoskeletal movement using OpenSim and MATLAB*. PeerJ, 2016. **4**: p. e1638.
70. Pandy, M.G., F.C. Anderson, and D.G. Hull, *A parameter optimization approach for the optimal control of large-scale musculoskeletal systems*. 1992.
71. Falisse, A., et al., *Rapid predictive simulations with complex musculoskeletal models suggest that diverse healthy and pathological human gaits can emerge from similar control strategies*. Journal of the Royal Society Interface, 2019. **16**(157): p. 20190402.
72. Srinivasan, M., *Fifteen observations on the structure of energy-minimizing gaits in many simple biped models*. Journal of The Royal Society Interface, 2011. **8**(54): p. 74-98.
73. Hamner, S.R., A. Seth, and S.L. Delp, *Muscle contributions to propulsion and support during running*. Journal of biomechanics, 2010. **43**(14): p. 2709-2716.
74. De Groote, F., et al., *Evaluation of direct collocation optimal control problem formulations for solving the muscle redundancy problem*. Annals of biomedical engineering, 2016. **44**(10): p. 2922-2936.
75. Koelewijn, A.D., D. Heinrich, and A.J. Van Den Bogert, *Metabolic cost calculations of gait using musculoskeletal energy models, a comparison study*. PloS one, 2019. **14**(9).
76. Gualdi-Russo, E., *Sex determination from the talus and calcaneus measurements*. Forensic science international, 2007. **171**(2-3): p. 151-156.
77. Lichtwark, G. and A. Wilson, *Is Achilles tendon compliance optimised for maximum muscle efficiency during locomotion?* Journal of biomechanics, 2007. **40**(8): p. 1768-1775.
78. Lichtwark, G., K. Bougoulias, and A. Wilson, *Muscle fascicle and series elastic element length changes along the length of the human gastrocnemius during walking and running*. Journal of biomechanics, 2007. **40**(1): p. 157-164.
79. Fletcher, J.R., S.P. Esau, and B.R. MacIntosh, *Changes in tendon stiffness and running economy in highly trained distance runners*. European journal of applied physiology, 2010. **110**(5): p. 1037-1046.
80. Ueno, H., et al., *Relationship between Achilles tendon length and running performance in well-trained male endurance runners*. Scandinavian journal of medicine & science in sports, 2018. **28**(2): p. 446-451.
81. DeSilva, J., et al., *One small step: A review of Plio-Pleistocene hominin foot evolution*. American journal of physical anthropology, 2019. **168**: p. 63-140.
82. Prang, T.C., *Calcaneal robusticity in Plio-Pleistocene hominins: Implications for locomotor diversity and phylogeny*. Journal of human evolution, 2015. **80**: p. 135-146.